LANGLEY
GRANT
IN-33-CR
252517
REPRINTS
REMOVED
72 P.

THEORETICAL AND MATERIAL STUDIES OF THIN-FILM ELECTROLUMINESCENT DEVICES

Final Report

Project No. A-4168

NAG1-586

Prepared for:

Dr. J. B. Robertson/494
NASA
Langley Research Center
Hampton, VA 23665

Prepared by:

Dr. C. J. Summers
Georgia Tech Research Institute
and Microelectronics Research Center
Georgia Institute of Technology
Atlanta, GA 30332

March 1989

(NASA-CR-186104) THEORETICAL AND MATERIAL STUDIES OF THIN-FILM ELECTROLUMINESCENT DEVICES Final Report (Georgia Tech Research Inst.) 72 p
CSCL 09A
N90-14468
G3/33 Unclas 0252517

THEORETICAL AND MATERIAL STUDIES OF THIN-FILM ELECTROLUMINESCENT DEVICES

Final Report

Project No. A-4168

Prepared for:

Dr. J. B. Robertson/494
NASA
Langley Research Center
Hampton, VA 23665

Prepared by:

Dr. C. J. Summers
Georgia Tech Research Institute
and Microelectronics Research Center
Georgia Institute of Technology
Atlanta, GA 30332

March 1989

TABLE OF CONTENTS

		Page No.
1.	Introduction	1
2.	Background	4
3.	Progress	9
	3.1 Review	9
	3.2 High Field Electronic Transport in ZnS and ZnSe	11
	3.3 The Variably Spaced Superlattice Energy Filter	16
	3.4 Application of VSSEF Structures to Advanced Device Concepts: The Avalanche Photodiode and Electroluminescent Device	22
	3.5 Molecular Beam Epitaxial Growth Studies	26
	3.6 MBE of ZnS on Si	27
	3.7 Chemical Beam Epitaxy System Development	50
4.	Conclusion	57
5.	Technical Presentations and Publications	61
6.	Technical Personnel	63
7.	References	64
8.	Appendix A	66

LIST OF FIGURES

NUMBER	DESCRIPTION	PAGE NO.
Fig. 1.	Schematic of thin-film electroluminescent device.....	5
Fig. 2.	Illustration of operation of thin-film electro-luminescent device, depicting hot electron and impact exication processes.....	6
Fig. 3.	Energy band structure for dc-electroluminescent device at zero bias and under bias...	8
Fig. 4.	Electron energy distribution function calculated from the ensemble Monte Carlo simulation with the electric field as a parameter. The distribution function is divided by the density of states function giving the probability density as a function of energy. The distrubtion is sharply peaked at low energies due to the very small density of states there.....	14
Fig. 5.	The electron energy distribution calculated from the ensemble Monte Carlo simulation at various electric field strengths. The distribution is divided by the density of states function. Due to the very small density of states at low energies, the distribution if greatly peaked there.....	15
Fig. 6.	The Variably Spaced Superlattice Energy Filter (VSSEF) device.....	17
Fig. 7.	A three-well VSSEF structure designed for electron injection at a voltage of 0.2V.....	19
Fig. 8.	I-V characteristics obtained for a three-well VSSEF structure.....	21
Fig. 9.	Transmissivity versus incident electron energy for a VSSEF design for a 1.55 μm APD using CdMnTe (E_{G2} = 2.0 eV) barriers and HgCdTe (E_{G1} = 0.8 eV) QWs, m* (CdMnTe) = 0.1 m_o, m* (HgCdTe) = 0.05 m_o.....	24

LIST OF FIGURES
(Continued)

NUMBER	DESCRIPTION	PAGE NO.
Fig. 10.	Transmissivity versus incident electron energy for a VSSEF design for electron injection at 2.7 eV for electroluminescent applications. The structure's parameters are given in ref. 23	25
Fig. 11.	Oxide desorption study for sample 87-14	35
Fig. 12.	Oxide desorption study for sample 87-8	36
Fig. 13.	RHEED studies for Layer 87-B	40
Fig. 14.	Streak Broadening Occurs as Growth Progresses.	43
Fig. 15.	Twin Spots in a Single Crystal RHEED Pattern..	44
Fig. 16.	Twin Spots in a Polycrystalline RHEED Pattern.	45
Fig. 17.	Twinning in a ZnS Film Growing on a Si(111) Substrate	46
Fig. 18.	Schematic of Development Chemical Beam Epitaxy System	51
Fig. 19.	Vapor Pressure of Sulphur Species of Molecular Beam Epitaxially Grown ZnS	54
Fig. 20.	Schematic of CBE Gas Delivery System	55

LIST OF TABLES

TABLE NO.	DESCRIPTION	PAGE NO.
Table 1.	Experimental Parameters of First Set of ZnS Growth Runs (Set 87-)	28
Table 2.	Simplified Cleaning Procedure	33
Table 3.	Experimental Parameters for Second Set of ZnS Growth Runs. Desorption Temperature, Substrate Temperature and Flux	41

1. INTRODUCTION

This program was formulated to address the need for better color displays in aircraft and space shuttle work stations as well as many applications for these devices in industry, commerce, and entertainment. At present these needs are satisfied by the cathode ray tube (CRT) and in some limited situations by light emitting diodes (LED's) and liquid crystal devices (LCD's). Unfortunately, the latter two devices are severely limited in their color capabilities. For example, there is no viable blue LED available, and LCD's can only offer a change in contrast. However, these devices do have significant advantages; they can be operated at low voltages, can be made as thin panels and thus, are compatible with integrated circuits and their fabrication technology. Also, these devices are extremely rugged, long lived, and light. All of these advantages makes them ideally suited for aerospace applications and in situations where a flat display screen is desirable. In contrast, the cathode ray tube is a high voltage relatively bulky device, and requires supporting electronics which add significantly to its size and weight. In addition, for high contrast applications and in adverse environments, its operating lifetime is limited. However, its display capabilities, color and screen size, are unmatched by any other type of device which accounts for its dominance of this market for the last three decades.

Recently, there has been a renewed interest in both ac and dc thin-film electroluminescent display devices. Typical a.c. devices operate at intermediate voltages (200-300 volts), display all the primary colors (red, green and blue), can be fabricated as large area flat panels (8 x 8 inches), and have exhibited long lifetimes under adverse environments. Essentially, these devices consist of a thin semiconducting film which acts as the host for the luminescent center and provides the source of high energy electrons

to excite the center. The most common material system is ZnS:Mn which emits in the yellow region of the spectrum. The problem with these devices is that their efficiencies are low resulting in poor picture contrast, and it is difficult to accommodate different color centers in the same or compatible host lattices. Conventionally, these devices are grown by evaporation of amorphous undoped and doped layers which are then annealed to promote more efficient luminescent devices. dc electroluminescent devices also have been realized using metal-insulator-semiconductor, or metal-insulator-metal structures, or Schottky barriers. In these devices, the source of free charge carriers is the metal electrode. Through application of a reverse bias in a Schottky barrier device, electrons tunnel from the metal into the semiconductor. Similar tunneling of electrons through a very narrow insulator layer in metal-insulator-semiconductor devices leads to significant carrier injection. The principle advantge of dc electroluminescent devices over their ac counterparts is due to the much larger free-carrier concentration within the dc device available to impact excite the luminescent centers, i.e., Mn or comparable rare earths in the ZnS or ZnSe layers. The use of crystalline semiconductor films has also recently been shown to result in higher efficiencies. Comparable brightness devices operating at very low voltages (4-18V) have been developed by growing epitaxial ZnSe on n-type GaAs. The high performance characteristics are attributed to the high concentration of source electrons, the longer electron free path and higher radiative efficiencies in the crystalline ZnSe layer. If further improvements could be obtained, then these structures would stand a realistic chance of competing with CRT displays. Examination of the literature shows that quantitative knowledge of the mechanisms essential to efficient performance is not available for either non-crystalline or crystalline structures, and that few

correlations have been made between device performance and material purity, defect structure, and crystallinity.

This contract was directed toward obtaining a detailed theoretical and experimental understanding of the mechanisms required for the fabrication of high efficiency semiconductor dc electroluminescent display devices.

2. BACKGROUND

2.1 Physical Description of Device Operation

As shown by Figure 1, a typical thin film electroluminescent device is a symmetrical insulator-semiconductor-insulator sandwich which produces light when biased by a high electric field.[1] The key ingredient of the structure is the high resistivity semiconductor layer which contains the active luminescent center and is the medium for the transport of hot electrons. The most common conception of device operation is illustrated by Figure 2. At high electric fields electrons trapped at the first insulator-semiconductor interface are excited from these states and tunnel into the conduction band or the semiconductor.[2] Here they are accelerated (heated) further by the electric field so that they continue to gain energy. For high enough fields, the hot electrons gain sufficient energy to impact-excite the active luminescent center.[3,4] In this process the hot electron transfers its energy to an electron in the ground state of the atom, thus elevating it to an excited state. This causes a population inversion in the center which is reversed when the electron falls back to the ground state with the emission of a photon.[5,6] Thus, the electrical energy in the device is converted to light.

Those electrons which are not captured by the luminescent center traverse the structure and collect near the anode. This causes a positive space charge in the second insulator which hinders the transport of further electrons across the device. Consequently, the electron density across the semiconductor region decreases and the light output falls. However, if the polarity of the external voltage is suddenly reversed, the action of the reversed electric field in the device is two-fold. New electrons are injected into the device from the second semiconductor-

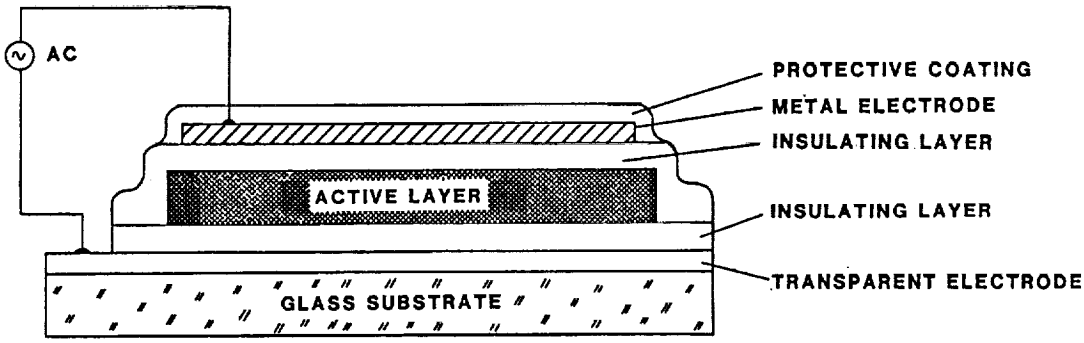

Figure 1. Schematic of thin-film electroluminescent device.

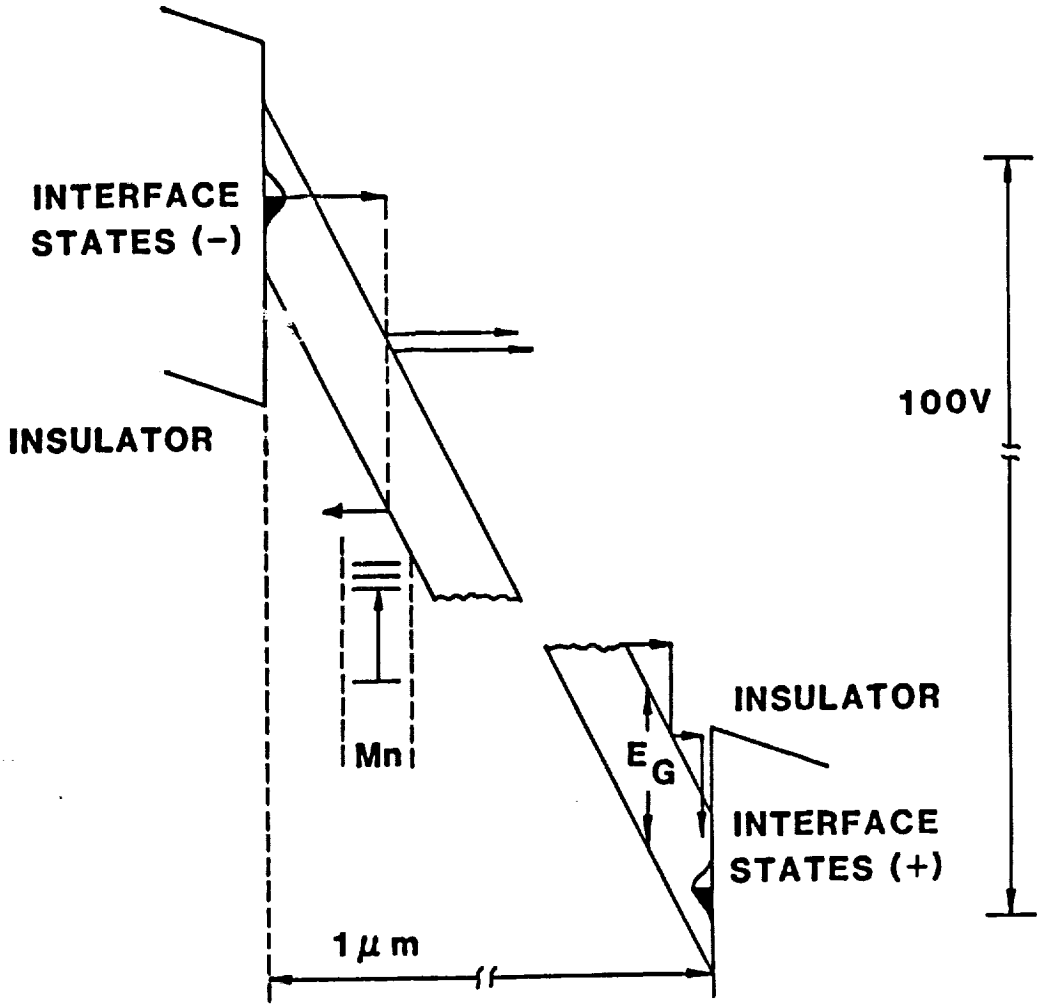

Figure 2. Illustration of operation of thin-film electroluminescent device, depicting hot electron and impact exication processes.

insulator interface, and these electrons and the electrons trapped near the second electrode are accelerated back into the semiconductor layer by the combined field due to the external applied voltage and the space charge. The increased electron population will thus produce a higher emission.[1] By alternately switching the voltage, increased light output can be obtained until the generation of electrons equals their loss by recombination processes in the structure.

Figure 3 shows the high performance dc electroluminescent device reported by Mishima et al.[7] under zero and operating bias conditions. Essentially, here the use of a high concentration of source electrons, and crystalline material has resulted in significantly lower operating voltages and higher efficiencies.

The efficiency of the device is thus dependent on the properties of the luminescent center, host lattice, and cladding insulator; and the way in which the device is operated. To optimize these devices therefore, a greater understanding is required of the physical mechanisms controlling carrier generation, charge transport and multiplication, the impact excitation process, the recombination properties of the luminescent center, and the functions of the insulating and contacting layers of the device.

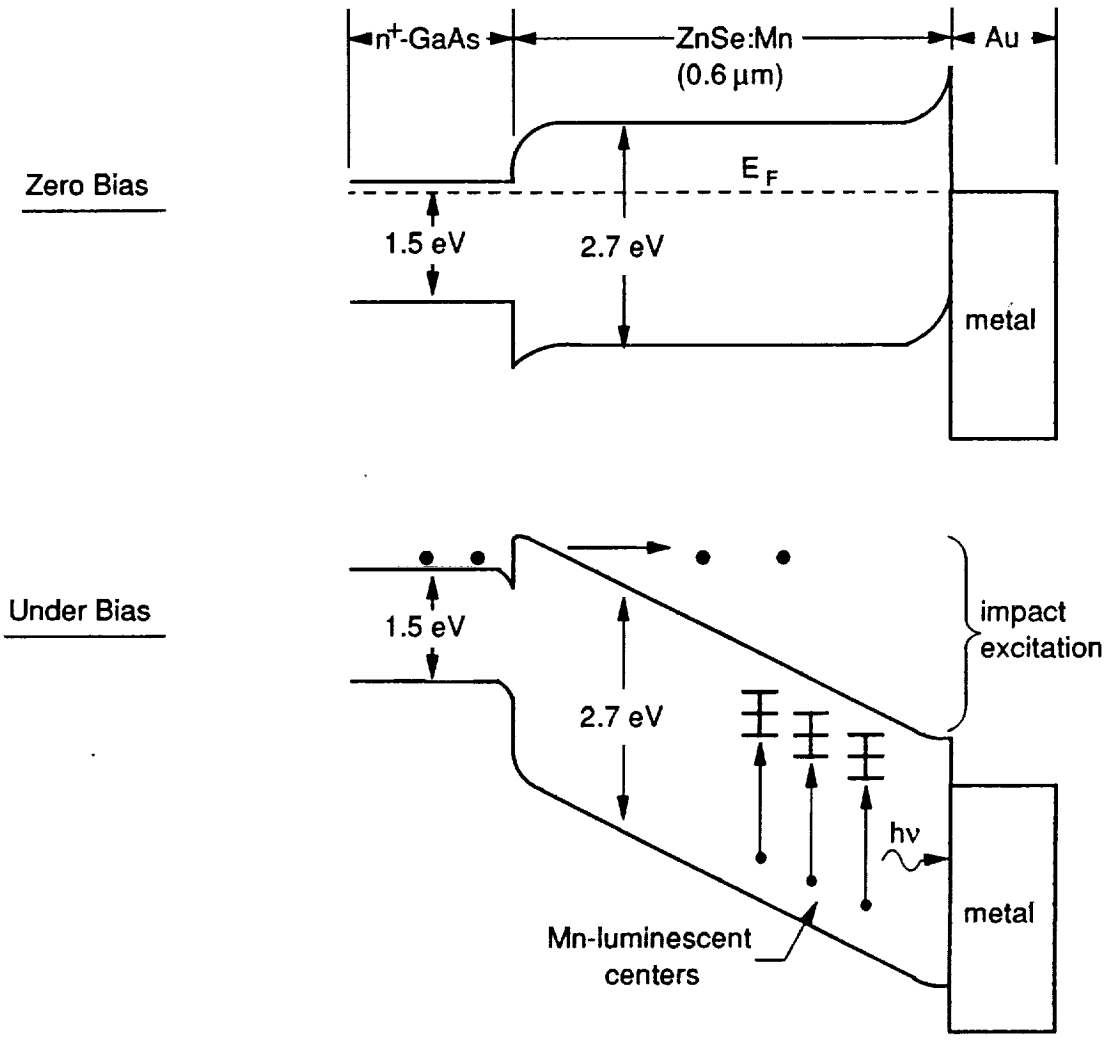

Figure 3. Energy band structure for dc-electroluminescent device at zero bias and under bias.

3. PROGRESS

3.1 Review

The initial phase of this work was to appriase and review the properties and performance characteristics of current thin-film electroluminescent devices. This showed that although sufficient information was known about each mechanism to give a qualitative description of each process, quantitative descriptions of the most important mechanisms were not available, either because of their complexity, or because they had not been studied in detail. The quality of the materials studied also severely limited precise measurements of many of the physical mechanisms controlling the performance characteristics of these devices. It was also apparent from this initial assessment made in 1985, that the Display Industry was intent on improving the performance of display devices by refining current technologies. This approach has shown some promising results by the development of some new phosphors and host lattice combinations with higher brightness and suggests that the commercialization of these devices may soon be possible. However, these devices still require a high voltage A.C. bias (~200V, 5 kHz) to obtain the required performance. It was also apparent that there was very little work directed at understanding in detail the physical mechanisms which control device operation.

This program was therefore directed to perform fundamental theoretical and experimental studies of electroluminescent materials and devices; such as in-depth theoretical investigations of the physical processes controlling device operation and the development of new device concepts. In parallel with these investigations, an experimental program to grow highly crystalline layers of ZnS and ZnSe doped with Mn and suitable rare-earth dopants was initiated in order to study the optical properties of

the luminescent centers and for prototype device structures evaluation.

As discussed previously, the performance of thin-film electroluminescent devices is very dependent on a number of complex and interacting physical mechanisms; specially the generation of hot electrons and the use of charge multiplication techniques to increase their density, the impact-excitation process, the recombination processes of the luminescent center, and the properties of the insulating and electrode films and interfaces between layers.

Currently, the quantum and power efficiencies are very low, typically less than 1% and 0.1%, respectively. These very low values result from the following problems.

1. The density of electrons transversing the active layer is very low, typically between 10^{10}-10^{11} cm^{-3}. This is because interface and deep levels provide a very limited and uncontrollable source of electrons and because at present it is difficult to obtain high multiplication factors in these structures.

2. The hot electron distribution is extended over a wide range of energies such that only a relatively small number of electrons have sufficient energy to impact-excite a luminescent center.

3. The electron impact-excitation cross-section of the centers is relatively small.

4. The radiative and non-radiative recombination mechanisms of the centers have not been fully documented and are unknown for high concentrations of luminescent centers.

Of the above factors, the generation of a high density of hot electrons represents a major limitation to the performance efficiency of a thin-film electroluminescent device. Therefore, the efficiency can be best improved by increasing the number of hot electrons with high enough energy capable of exciting a luminescent center.

To fully investigate this mechanism modeling, studies were performed of the hot electron distributions in ZnS and ZnSe obtained by the application of an electric field.[8] Also, a new concept, the variably spaced superlattice energy filter (VSSEF) was invented.[9] This concept we believe has significant benefits for thin-film electroluminescent displays because it provides high energy injection of near monoenergetic electrons into a bulk semiconductor layer at an energy tuned to the impact-excitation energy of the luminescent center. This should result in a dramatic increase in the efficiency and brightness of TFEL devices with the additional advantage of low voltage D.C. operation.

A brief description of the principal results of each of these investigations is given below. The complete description of the analyses, results and conclusions of this work is contained in the published papers resulting from these investigations which are contained in Appendix A.

3.2 High Field Electronic Transport in ZnS and ZnSe

Previous theoretical investigations of electron transport in bulk ZnSe or ZnS have been confined to determining the low field mobility as a function of temperature and impurity concentration.[10,11] These investigations have done much to clarify the nature of electronic and hole transport in bulk ZnSe but have not probed the physics of very high field transport in these materials at which electroluminescence occurs.[12] In fact, all of the previous models rely on an effective mass formulation as well as a first order treatment of the electron-phonon scattering rates. It is well known that both of these approximations fail at high carrier energies. Therefore, a different approach must be used to study the nature of the high field carrier distribution functions.

We therefore theoretically investigated the nature of electronic transport and the high energy tails of the electron

distribution functions in bulk ZnSe and ZnS as a function of the applied electric field using a model particularly well tailored to very high field strengths. The calculations include the full details of the first two conduction bands as well as the full order treatment of the electron-phonon scattering mechanisms. The steady state electron drift velocities as a function of applied electric field were determined for each material system as well as the total electron-phonon scattering rates. In addition, the high field probability distribution function was calcualted for both ZnS and ZnSe, figures 4 and 5. These studies showed that the electron distribution function is predicted to be significantly cooler in ZnS than in ZnSe at comparable electric fields. Specifically, at 500 kV/cm, no carriers in ZnS survive to energies at which impact excitation processes can occur, ~2.3 eV. In fact, no electrons attain even 2.0 eV in energy. Conversely, in bulk ZnSe, a significant fraction of electrons, ~2-3%, attain energies greater than or equal to 2.3 eV. The cooler distribution in ZnS is due predominantly to the much greater electron scattering rate, roughly twice as large as in ZnSe, within the gamma valley. Therefore, the electrons are more greatly confined within the gamma valley at comparable field strengths leading to an overall cooler distribution. This is clearly reflected as well by the greater threshold field in ZnS than in ZnSe. The larger gamma valley scattering rate in ZnS is due to the much greater polar optical phonon energy and carrier effective mass. In addition, the electron scattering rate is somewhat higher in ZnS than in ZnSe at energies above the intervalley threshold. Again, this acts to cool the carriers within the ZnS more than in the ZnSe.

Due to the much cooler electron distribution in ZnS, the threshold field for electroluminescence, which is a measure of the number of electrons at energies at which impact excitation processes can occur, is greater than in ZnSe. Consequently, EL

displays made using ZnS will be less efficient than those employing ZnSe, since a greater input power is necessary to achieve comparable output brightness. In either case, display efficiencies are poor due to the difficulty in heating significant carriers to the impact excitation threshold energy. Therefore, under comparable conditions ZnS electroluminescent devices should have a sizeably greater threshold voltage than ZnSe devices. This is in accord with previous experimental observations of thin film ZnSe:Mn and ZnS:Mn EL displays.[13]

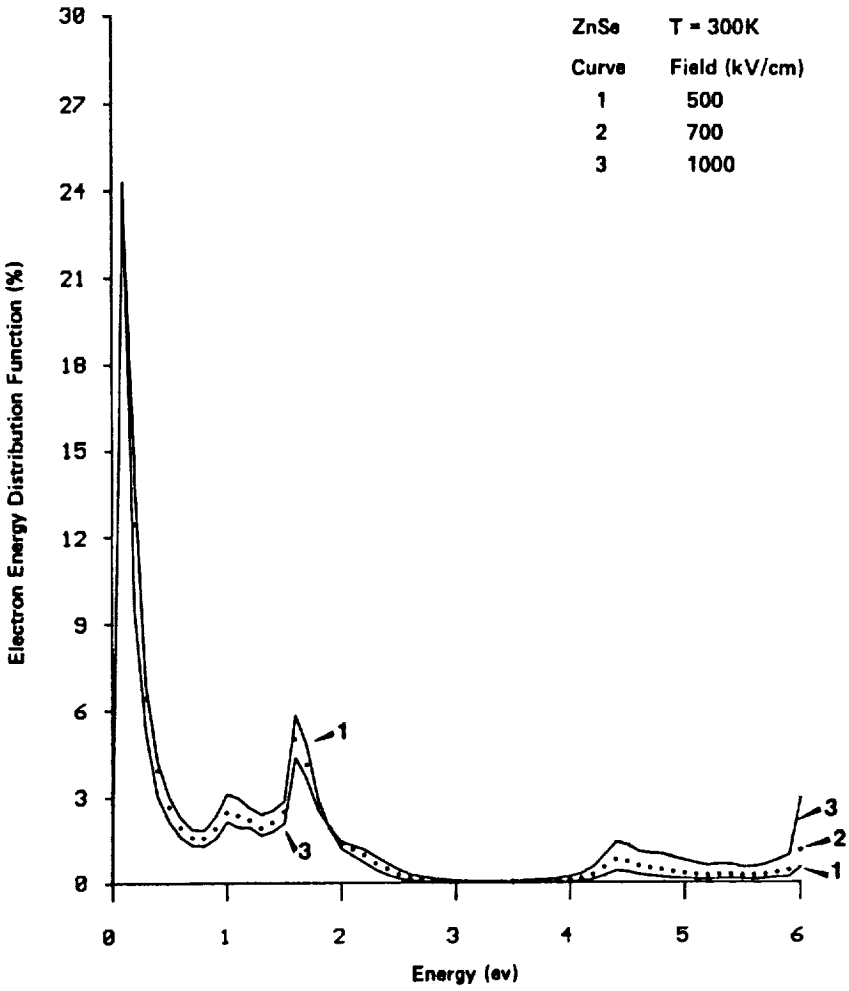

Figure 4. Electron energy distribution function calculated from the ensemble Monte Carlo simulation with the electric field as a parameter. The distribution function is divided by the density of states function giving the probability density as a function of energy. The distrubtion is sharply peaked at low energies due to the very small density of states there.

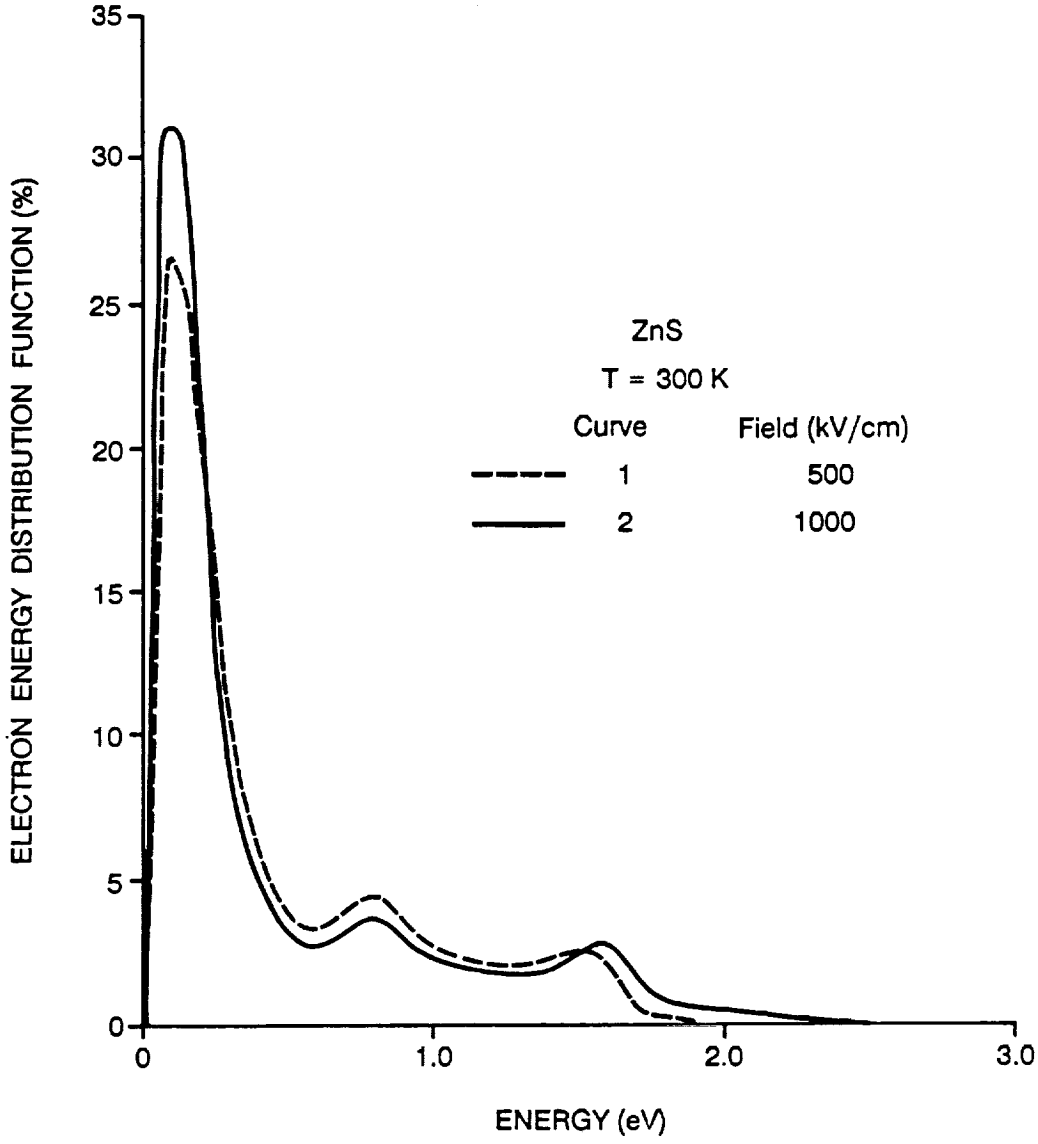

Figure 5. The electron energy distribution calculated from the ensemble Monte Carlo simulation at various electric field strengths. The distribution is divided by the density of states function. Due to the very small density of states at low energies, the distribution if greatly peaked there.

3.3 The Variably Spaced Superlattice Energy Filter

As demonstrated by the previous discussion, the performance of electroluminescent devices, and also avalanche photodiodes and ballistic transistors, depends critically upon the efficient production of high-energy electrons.[14-17] Performance of these devices is governed by threshold processes such as impact excitation or impact ionization in which carriers must attain a minimum energy in order to initiate the process. Carrier heating is typically accomplished through the application of an applied electric field. In steady state field heating is balanced, on average, by inelastic scattering events. The competing processes of field heating and phonon cooling results in only a very small fraction of the injected electrons attaining high energies. The high energy tail of the distribution function is quite small even at high applied electric field strengths. Therefore, devices which require high energy carriers suffer overall poor power efficiencies, since much of the input power is lost to inelastic phonon scatterings, rather than direct heating of the carriers.

Presently, there is great interest in single quantum well structures because their small dimensions coupled with the presence of negative differential resistance in the output current-voltage characteristic, enable the realization of very high frequency oscillators.[18,19] However, we have also proposed the use of resonant tunneling in multiple quantum well (MQW) structures to provide high energy carrier injection.[9,20] In our device scheme, called the variably spaced superlattice energy filter (VSSEF), the energy levels arising from spatial quantization effects become resonantly aligned under bias. By judiciously varying the well layer widths, and hence, the energies of the confined quantum states, the levels in adjacent wells are at zero bias effectively separated in energy by the voltage drop across each cell, thus resulting in their alignment under the appropriate bias voltage (Figure 6). Hence,

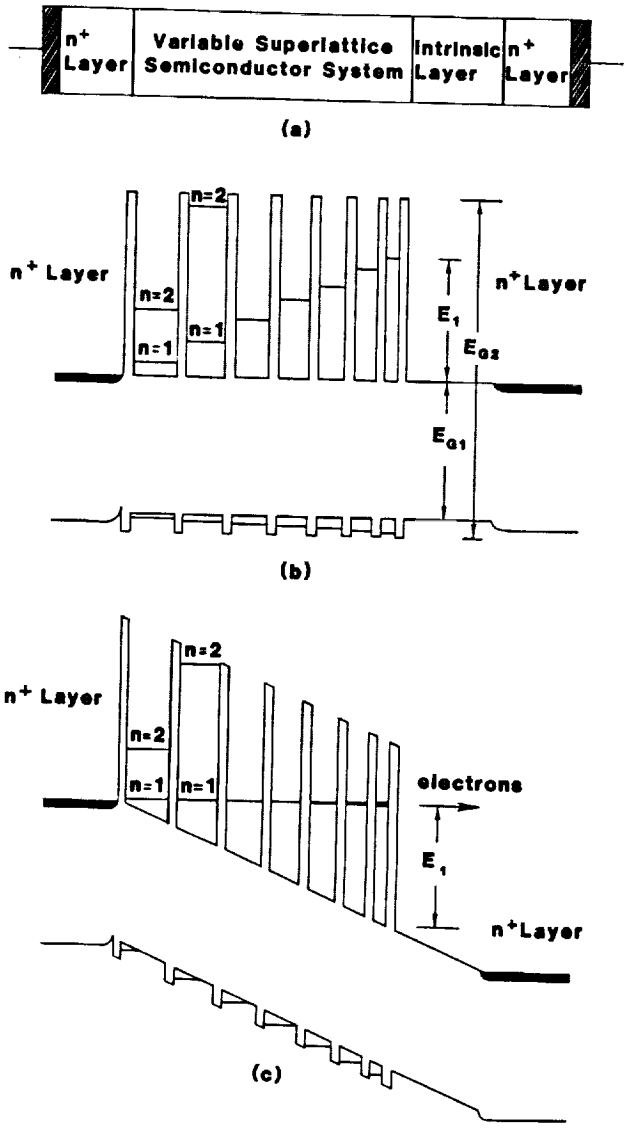

Figure 6. The Variably Spaced Superlattice Energy Filter (VSSEF) device.

electrons tunnel through the first potential barrier into the first quantum well of the superlattice and then continue to resonantly tunnel from one quantum well to the next. Thus, in the simplest implementation of the proposed scheme, electrons are injected into the conduction band of the active semiconductor layer at an energy above the conduction band edge equal to the band bending across the superlattice.

The variably spaced superlattice structures analyzed in these studies were designed using a self-consistent solution of the Poisson and Schroedinger equations under an applied bias. The solution of the Schroedinger equation is found first assuming a uniform applied electric field throughout the structure neglecting the self-consistent contribution from the carrier electric charge. The solution of the Schroedinger equation within each region is then given by a linear combination of Airy and complimentary Airy function.[9,20] The continuity of the wavefunction and its first derivative at each interface is then used to generate a series of 2 x 2 matrices which couples the incident wavevector to the outgoing wavevector in the heterostructure stack. The overall transmission coefficient for the system is then found which enables the determination of the steady-state electronic wavefunctions and electronic charge density. The Poisson equation is solved for the self-consistent electric field. The Schroedinger equation is again solved in each region, with the final solution found recursively. In this way, different multiple well structures can be designed which show resonant alignment under an applied bias.

Using the above technique we designed a three well, four barrier variably spaced superlattice structure using $Al_{0.35}Ga_{0.65}As$ barriers and GaAs quantum wells which becomes resonantly aligned at a bias of 0.2 volts (see Figure 7). Calculation of the transmissivity of the structure as a function of carrier energy indicates that for an incident carrier energy of 0.02 eV, that the

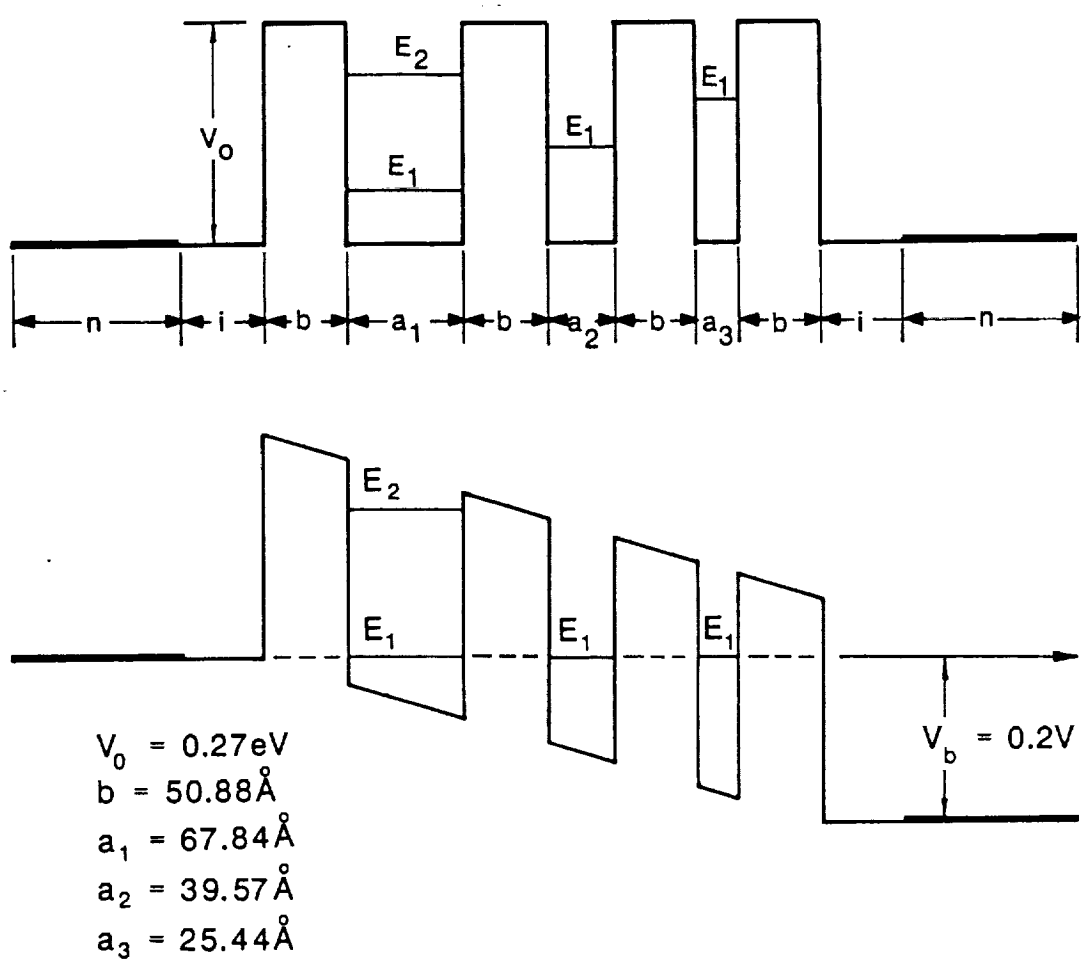

Figure 7. A three-well VSSEF structure designed for electron injection at a voltage of 0.2V.

transmission is close to unity. Therefore, it is expected that the negative differential resistance will occur at a bias of 0.22 volts, the sum of the resonant alignment bias, 0.02 volts, and the incident carrier energy, 0.02 eV.

The structure presented in Figure 7 was grown using a Varian GEN II molecular beam epitaxy system on a n^+ Si-doped (001) GaAs substrate. To minimize both space-charge and depletion effects, the barrier doping was reduced to relatively low concentrations. The actual device was fabricated by evaporating Au:Ge/Ni/Au metallization layers, and ohmic contracts were formed by alloying at 380°C for 2 minutes in an inert atmosphere. An overlayer of 1 um of Au was used to increase the structural integrity of the device. Mesas 20-50 um in diameter were defined using conventional photolithic techniques, and 0.7 mil Au leads were bonded to the top surface using a low-pressure bonding procedure.

The resulting current-voltage characteristics for the three well devices are presented in Figure 8 as a function of temperature. As the temperature is decreased down to below 100K, the peak-to-valley ratio exhibits little further temperature dependence. It is important to realize that the NDR occurs at a bias voltage of ~0.24 volts in excellent agreement with that predicted from the theory stated above. Therefore, the observed experimental resonances, their independence of temperature, and the very close correlation obtained with theory unambiguously confirm the presence of resonant tunneling within this three well, four barrier structure. This experiment was the <u>first</u> observation reported of resonant tunneling in a multiquantum well structure consisting of three variable width wells.[21,22]

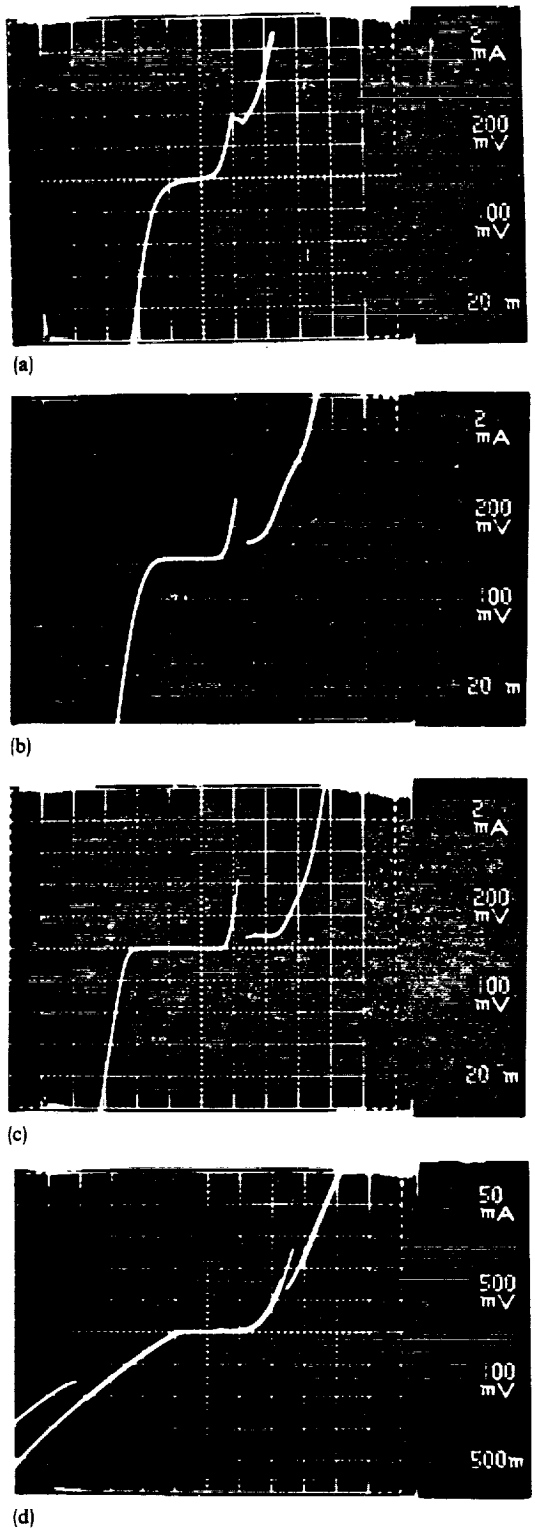

Figure 8. I-V characteristics obtained for the three-well 0.2V VSSEF structure shown in Figure 7 at temperatures of (a) 200, (b) 100, (c) 10 and (d) 50K at higher bias.

ORIGINAL PAGE
BLACK AND WHITE PHOTOGRAPH

3.4 Applications of VSSEF Structures to Advanced Device Concepts: The Avalanche Photodiode and Electroluminescent Device

To explore the limits of the VSSEF structure we have also performed calculations for both avalanche photodiode and electroluminescence device structures.[23] For the photodiode structure we assume a device with E_{G1} = 0.8eV and E_{G2} = 2.0eV which has application to the fabrication of highly efficient APDs operating at 1.55 μm. Structures with these properties should be obtainable by using a CdMnTe alloy for the high bandgap material and a $Hg_{0.38}Cd_{0.62}Te$ alloy for the low bandgap semiconductor. With this energy band scheme the VSSEF structure essentially emulates the staircase structure proposed by William et al.[24] By using a series of VSSEF stages, impact ionization can be produced in a spatially deterministic manner, thus achieving gain with the lowest possible excess noise contribution. The transmissivity versus incident electron energy plots of two possible structures designed for this application are shown in Figure 9 and demonstrate that significant tunneling transmissivities can be obtained for barrier widths of 35 and 25Å and QW widths ranging between 89 and 14A. These structures were designed using 3 QWs whose widths were chosen to align the n = 1 levels under a bias of 0.8V. The layer thicknesses used are well within the experimental capabilities of MBE growth techniques and, obviously, with more refinement, the structure can be optimized to give near unity transmission probabilities.

As a further demonstration of the potential of this concept, Figure 10 demonstrates the possibility of achieving electron injection at 2.7eV so as to achieve blue luminescence in an EL device. The structure is, again, a 3-QW design and assumes barrier widths of 10Å with potential barriers of 1.0, 2.0, 4.0 and 4.0eV, respectively. It is assumed that the barrier effective mass is $0.5m_0$, where m_0 is the free electron mass. The QW material is

assumed to be ZnSe, with E_{G_1} = 2.7eV and an electron effective mass of $0.17m_0$. By designing for n = 1 level alignment under a 2.7V bias, as shown in Figure 10a, significant transmissivities are achieved for QW widths of 26, 6.3 and 6.0Å, respectively. The small QW widths and high electric field make this an impractical scheme, but Figure 10b demonstrates that a significantly more practical structure can be achieved by aligning with the n = 2 level in the third QW. For an electron concentration of 10^{18} cm^{-3} in the left hand electrode, current densities of $10^{14}A/cm^2$ are calculated for this structure. Although speculative, this design demonstrates that the essential physics is correct. Possible material systems for this structure are the $ZnSeS:CaSrF_2$ ternary alloys which can be well lattice-matched and in which large conduction band discontinuities are possible because E_{G_2} can range between 11.44 and 12.2eV.

It should also be noted that the width of the resonantly aligned channel in Figures 9 and 10 is less than or comparable to the optical phonon energy for these materials. Thus, electron scattering in the aligned states is expected to be small.

In summary, we have developed a theoretical treatment for a variably spaced superlattice in an electric field and demonstrated that its transport properties under bias are similar to the Tsu and Esaki SL. However, because it provides an efficient mechanism for high energy electron injection in which a stream of hot monoenergetic electrons can be created and tuned to specific injection energies, this structure has many significant applications. Further work investigating the potential applications of the VSSEF concept in optical and infrared avalanche detectors, electroluminescent devices and IMPATT and negative resistance devices is in progress.

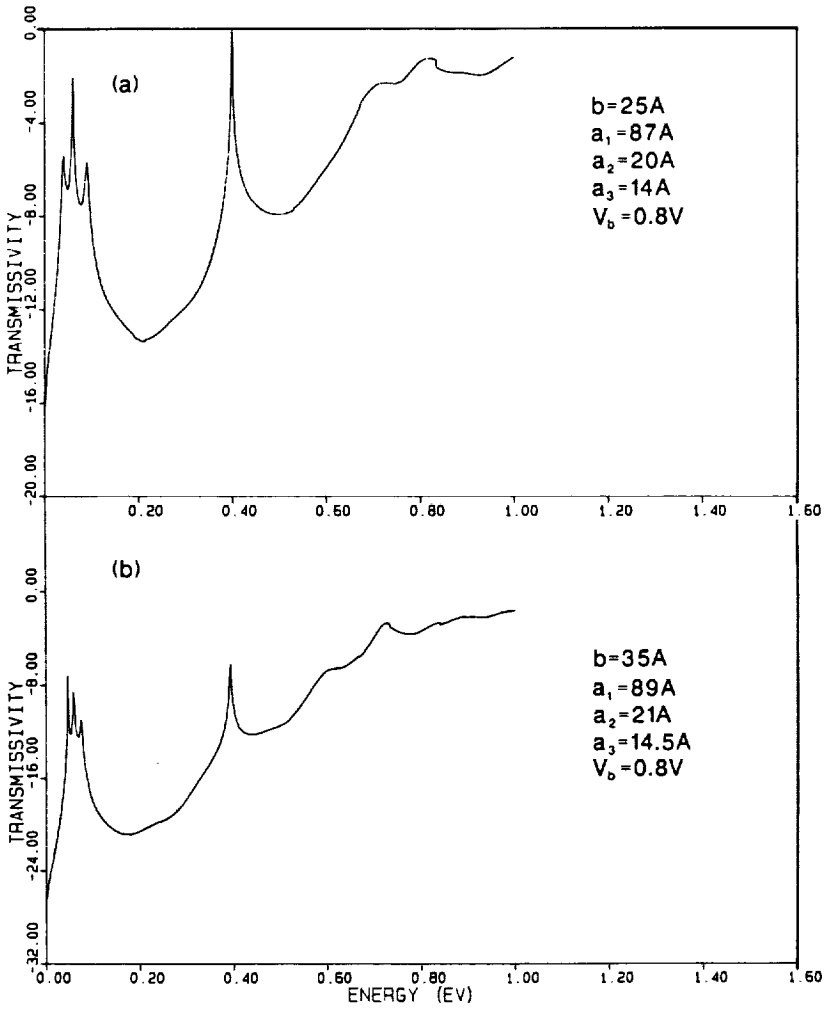

Figure 9. Transmissivity versus incident electron energy for a VSSEF design for a 1.55 μm APD using CdMnTe (E_{G2} = 2.0 eV) barriers and HgCdTe (E_{G1} = 0.8 eV) QWs, m* (CdMnTe) = 0.1 m_0, m* (HgCdTe) = 0.05 m_0.

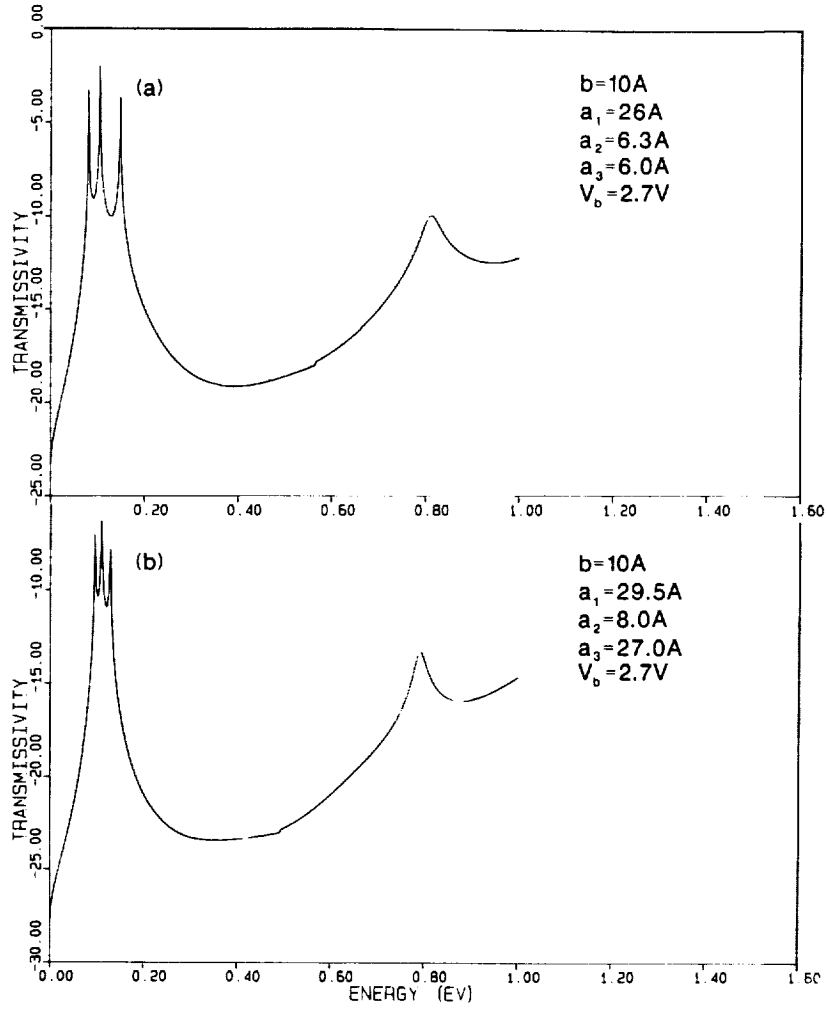

Figure 10. Transmissivity versus incident electron energy for a VSSEF design for electron injection at 2.7 eV for electroluminescent applications. The structure's parameters are given in ref. 23.

3.5 Molecular Beam Epitaxial Growth Studies

As discussed previously, the growth of crystalline ZnS layers on foreign substrates offers the potential to fabricate thin-film electroluminescent devices which can easily be incorporated into integrated circuit fabrication technologies. ZnS is a direct bandgap material, having the largest bandgap among the semiconducting II-VI compounds. This large bandgap makes it the most promising material for blue light-emitting diodes and other optoelectronic devices in the short wavelength region. ZnS crystallizes in the cubic phase below 1020°C at atmospheric pressure, with a lattice constant close to that of Si from room temperature to a few hundred degrees Celsius, the lattice mismatch being only -0.4%. This fact, in addition to the low cost and high quality of commercial silicon wafers, makes silicon preferable to GaAs as a substrate upon which to grow and fabricate devices based on thin epitaxial films of ZnS. Also only Si and GaAs possess all of the substrate properties needed for this type of structure. Thus, the initial ZnS layers were grown by MBE on both GaAs and Si substrates. Surprisingly, the best results were obtained on GaAs even though Si is more ideally lattice-matched to the ZnS lattice. The problems associated with growth on Si were attributed to the surface preparation which required a high temperature treatment above 1000°C to remove all of the surface oxide.

Because of this problem, the first series of growth runs were performed on (001) GaAs layers. In this work, techniques were developed to obtain very clean growth surfaces and to relieve the 4.5% lattice mismatch between ZnS and GaAs. The results of this work are described in detail in a publication entitled "Molecular Beam Epitaxial Growth and Structural Characterization of ZnS on (001) GaAs," which is duplicated in Appendix A. Thus, this work will not be repeated here, and the discussion will focus on the progress made in the MBE growth of ZnS on Si and the development

of a chemical beam epitaxy system for growing high quality electroluminescent structures on this substrate material.

3.6 MBE of ZnS on Si

This set of experiments was designed to investigate the effects of several parameters on the quality of thin films of ZnS grown by MBE on chemimechanically polished <100> silicon wafers. Specifically, effects of surface treatment, substrate temperature and beam flux were varied to produce a matrix of growth conditions. Substrate temperatures ranged from 200°C to 340°C. Beam fluxes ranged from 1.2 to 11.0 x 10^{-7} Torr. For growth of ZnS on <100> Si, it has been shown that the best results have occurred for a substrate temperature of 340°C, and a molecular beam in which $J_{Zn} = J_S$. A summary of the experimental parameters for each run is shown in Table 1.

The experiments were performed in a Varian Gen II system containing ion, Ti sublimation, and Vacsorb pumps. System base pressure was routinely in the low 10^{-10} Torr range without LN_2 flowing. With LN_2 flowing, system base pressure could be reduced to the high 10^{-11} Torr range before the cryoshields were heated by the substrate heater, and the base pressure limited by the operating conditions. By the time the substrate heater and source ovens had equilibrated, system pressure was between the low to high 10^{-9} Torr range.

The research goals were to: 1) find a surface preparation procedure that will grow a thin oxide yet protect the etched surface from carbon contamination, 2) find a low-temperature desorption technique that removes all the oxide, and 3) find the substrate temperature and beam flux that yield the best films as determined by RHEED, X-ray diffraction and photoluminescence.

Table 1. Experimental Parameters of First Set of ZnS Growth Runs (Set 87-)

EXP.	CLEANING PROCEDURE	FINAL DESORP. TEMP(C)	TIME @ TEMP (MIN)	Tsub @ FOR GROWTH	FLUX INIT./FINAL (x10-7 TORR)	GROWTH TIME	THICKNESS (A)	GROWTH RATE (A/HR)	RHEED @ END	COMMENTS
1	4-step	1000	15	270	5.7	56 MIN			SPOTTY	TWINNING
2	4-step	950	41	280	7.0/6.5	2 HRS 30 MIN			SPOTTY	TWINNING
3	Degrease, UVOCS,HNO3, UVOCS	940	1 HR 10 MIN	340	5.5/4.2	3 HRS 44 MIN			D-S RINGS VISIBLE	
4	4-step UVOCS after step #1	900	15	340	5.3/5.2	3 HRS 30 MIN			STREAKY, CONTRAST VARIATION	ROUGH SURFACE
5	4-step	825	1 HR 10 MIN	320	5.4/4.7	4 HRS 30 MIN			STREAKY, CONTRAST VARIATION	FLUX TOO LOW, TEMP TOO HIGH
6	4-step HNO3 etch 3 x only	900	1 HR 30 MIN	320	5.2/4.6	3 HRS 30 MIN			STREAKY, CONTRAST VARIATION	DUE TO TEMP PULSES
7	4-step	800	20	280	4.2	2 HRS 18 MIN	7750	3370	STREAKY, BUT FAINT	DUE TO FILM CHARGING
8	4-step	950	15	240	5.5/4.9	3 HRS 30 MIN			GOOD, UNIFORM CONTRAST	
9	DI,UVOCS,HF DIP,BOILING HCl, DI	950	30	200	6.2	3 HRS 30 MIN			NONE VISIBLE	DUE TO FILM CHARGING
10	SAME AS 87-9	950	18	280	5.2	3 HRS 37 MIN			STREAKY, CONTRAST VARIATION	
11	SAME AS 87-9	950	49	240	2.5/2.6	7 HRS			GOOD, UNIFORM CONTRAST	
12	SAME AS 87-9	900	30	240 @+5 MINS	11.0/7.0	3 HRS 30 MIN	12700	3629	UNIFORM AFTER 15 MIN	FILM CHARGING
13	SAME AS 87-9	800	20	200	1.2 @+10 MINS: 7.2/4.6	3 HRS 30 MIN	13500	3857	UNIFORM AFTER 30 MIN	FILM CHARGING

Substrate Mounting

The appropriate method for holding a Si substrate is important in guaranteeing even substrate heating and in affecting oxide desorption. For substrates such as GaAs or CdTe, whose oxide desorption temperatures are 582°C[24] and ~300°C, respectively, the surface tension produced by liquid indium is sufficient to bond these substrates to a solid molybdenum block. Indium evaporates rapidly at temperatures around 800°C, making it unsuitable for use with a silicon substrate. In our initial work substrates slid off the molybdenum mounting block upon approaching silicon oxide desorption temperatures. The molybdenum block was therefore modified to accommodate 2-inch wafers and eliminate the need for indium.

The initial modifications involved the machining of a large hole in the center of the block, essentially reducing the block to a thick annulus. A ledge of depth 0.013" is formed to accommodate a 2"-diam. wafer. The outer diameter of the ledge was therefore 2.003" (The entire moly block has a diameter of 2.25".), and the inner diameter was 1.75". Three pairs of holes were drilled 120 degrees apart; halfway between the tantalum holder retainer pins. The hole diameters were 0.020" and each pair was separated by 1/8". The wafer was restrained by a thin annulus of molybdenum sheet (0.010") with an outer diameter of 2.25" (same as the moly block), and an inner diameter of 1 7/8". Three pairs of holes are drilled to match the moly block. Thin gauge molybdenum wire (diam: 0.010") was used to tie the ring to the block.

The heat path for raising the temperature of the substrate was now no longer conduction from the solid moly block through the indium, but direct radiative heating from the resistance heaters to the backside of the substrate surface. It is therefore desirable to have the highest absorption coefficient for the incident radiation. For silicon substrates, a macrostructuring technique from the solar cell industry was used to produce

tetrahedral structures on the order of 5-12 microns high.[25] The procedure, essentially a preferential etch, was: (1) clean in hot trichloroethylene followed by methanol dip, (2) coat front surface with black wax for protection, (3) 5 minutes in a solution of D.I. water and NaOH (10% by weight), (4) dip wafer in D.I. water, (5) 5 minutes in a solution of D.I. water and NaOH (1% by weight), (6) rinse in hot D.I. water. Steps 3 and 5 were performed in an ultrasonic agitator to increase etch rate and remove hydrogen bubbles that form at the surface and which would otherwise inhibit further etching. Though the above procedure was successfully duplicated, it was found that in practice the matte finish on the back of the wafer made the texturing operation unnecessary.

A further improvement of the substrate mounting technique involved inserting a pyrolitic boron nitride (PBN) disk (0.020" thick) between the wafer and the heater coils. This necessitated milling out the ledge of the substrate holder to a depth of 0.033" to accommodate a 0.013"-thick wafer. In addition, the molybdenum retaining ring was replaced by molybdenum wire clips. This reduces the conductive heat path losses and levels the temperature distribution across the wafer. The PBN disk should also increase the accuracy of any pyrometric temperature measurement.

Essentially, the PBN served as a "heat-leveler." This material is designed to have a coefficient of thermal conductivity 30 times greater in the radial and circumferential directions than in the direction perpendicular to the surface. Heat-leveling was necessary due to Varian's 4-coil substrate heater design. In this configuration, a receptacle on the back of the solid molybdenum block isolates the tip of the thermocouple, which protrudes slightly from a protective ceramic sheath, from the direct radiation of the heaters. The temperature signal is, therefore, due to the tip being in mechanical contact with the block. In the modified configuration, the thermocouple tip was in contact with

the PBN disk, but was not shielded from the 4 heater coils surrounding it. Thus, the thermocouple was heated radiatively from both the heaters and by re-radiation from the back of the wafer. This introduces some uncertainty into the thermocouple reading. Ideally, the temperature should be measured by a pyrometer looking through a sapphire window on the front side of the wafer surface. Though an instrument sensitive enough to make measurements in the range of interest was not available, a calibration with an IRCON Modline "V" Series pyrometer was made. The instrument was designed to function in the 400°C to 1000°C range. It was found that the thermocouple readings differed by as much as +38°C at 400°C to -125°C at 975°C. In fact, the difference between the pyrometer and thermocouple readings was 5°C or less only between 550°C and 625°C. Between 200°C and 340°C, the range of growth temperatures of interest, there may be significant error from the true temperature. Therefore, the results presented here must be viewed in the context of relative temperature measurements.

Surface Cleaning

In cleaning the silicon <100> substrates, two basic approaches were used with minor variations. The first approach used a four-step RCA cleaning procedure.[25] The only variations in this procedure was to either repeat the final step - the HCl etch/HF dip, or to insert the wafer in the ultra-violet/ozone cleaning system (UVOCS) after the first step. This latter variation was attempted, but the resulting surface showed many particles and/or much damage. This may have been due to impurity desorption from the stainless steel wall interior of the UVOCS chamber.

The former variation: repetition of the fourth step, seemed most effective at yielding, bright 2-fold reconstruction during oxide desorption. The aforementioned procedure, while effective for cleaning, may cause surface damage and increase surface roughness. The second and more simple procedure described in Table 2 was also used. This procedure minimizes wafer handling, and any

anisotropies that may result from chemical processing, and prevents damage due to ultrasonic treatment. This procedure produced results comparable to that of the 4-step method. Thus, the surface cleaning method had a strong influence on the thickness of the surface oxide.

Oxide Desorption

The second most critical factor in preparing the surface for deposition was the manner in which the oxide was desorbed. Oxide desorption was performed by a two-step process. First, the substrate was baked out in the loadlock at 300°C, between 2 to 4 hours. This was followed by a transfer of the substrate from the loadlock through the transition tube to the growth chamber for thermal cleaning. Since the last step in the 4-step cleaning procedure was designed to grow a thin, protective oxide, subsequent oxide removal by thermal cleaning was strongly dependent on this bakeout. Oxide desorption times varied from a few minutes for very thin layers to over an hour for thick layers (>50 A).[26] In general, it was found that no matter how low the temperature was when the oxide began to desorb (as evidenced by the transition to a 2x2 reconstruction) the best results were obtained when the surface was left at the maximum temperature achievable for a reasonably long period (30 minutes or more). The maximum temperature achievable in our system was, given the inaccuracy of the thermocouple, approximately 950°C. Figure 11a-c (from experiment 87-14) shows the appearance of a 2x2 reconstruction beginning as low as 600°C, and becoming fairly pronounced at 800°C.

There are several problems that may occur during oxide desorption. First, it is not known to what extent the silicon surface experiences slip when the surface is held at 950°C from 30 to 90 minutes. For this reason, several attempts were made to grow on substrates that were kept below the maximum temperature.

Table 2. Simplified Cleaning Procedure

1. Rinse in overflowing deionized water for 10 min.
2. Expose for 5 min. to Ultra-violet Ozone Cleaning System (UVOCS) to remove organics.
3. Dip in 2.5% HF solution for 10-15 sec, to remove the oxide layer.
4. Boil in a solution of $HCl:H_2O_2:H_2O(3:1:1)$ at 90°C for 10 min. to make a thin surface oxide. (Mix HCl and H_2O together and bring to temperature. Just prior to use, add H_2O_2.)
5. Rinse in overflowing deionized water for 10 min.

These attempts were only made for substrates that exhibited the onset of oxide desorption at lower temperatures and which showed a fairly strong 2-fold reconstruction at 800°C. In particular, this was attempted in experiments 87-7 and 87-14. In the case of the former bright, 2x2 reconstruction was visible at only 700°C (see Figure 12). After the ZnS flux was initiated, a strong crystalline pattern remained visible (figures 12b-c). Here, the substrate had been at 800°C for about 30 minutes. In the case of the latter, the substrate had been left at 800°C for only 17 minutes when it was lowered to 600°C. The results were immediate and poor. The RHEED pattern indicated the surface was polycrystalline.

Second, it was not clear what reactions take place at oxide desorption temperatures. In experiment 87-5 the shutter to the ZnS oven was opened for about 15 seconds at 825°C. The RHEED pattern immediately degraded: twinning and/or surface roughness was apparent. Since this substrate never fully desorbed even after the shutter was closed and the substrate temperature (T_{sub}) raised from 825°C to 950°C, it is thought that carbides may have formed on the surface.

a) Transition to 2-fold at 600°C.

b) More pronounced at 750°C.

c) After 10 minutes at 800°C.

Figure 11. Oxide desorption study for sample 87-14.

ORIGINAL PAGE
BLACK AND WHITE PHOTOGRAPH

a) Maximum temperature: 800°C (Onset occurred at 700°C)

b) After 30 minutes desorption time at 800°C
T_{sub} = 280°C, flux initiated

c) RHEED after 1 hr. 50 min.

Figure 12. Oxide desorption study for sample 87-8.

ORIGINAL PAGE
BLACK AND WHITE PHOTOGRAPH

MBE Growth Techniques

After the oxide had been successfully removed, a bright (2x2) reconstructed surface was seen with RHEED, which indicated that the surface was prepared for growth. The substrate was then rotated out of position (facing away from the ovens) to minimize exposure to any contaminants or impurities from the source material, and its temperature (T_{sub}) was lowered to near the desired growth temperature before raising the temperature of the oven. This minimized the time between the point at which the growth flux level was achieved and the actual initiation of growth. Failure to do so resulted in a change from a (2x2) to a (1x1) reconstruction. As a result of raising the oven temperature, the growth chamber baseline pressure increased into the high 10^{-8} Torr range. This was unacceptable for high quality MBE growth and may have been the result of outgassing from the chamber walls due to the large heat load imposed by the source and substrate (both at roughly 1000°C). For this reason, the operation was phased such that the cryopump could handle the load due to outgassing. When T_{sub} dropped to about 50°C above the target substrate temperature, the ZnS oven was ramped from its idling temperature of 165°C to 1040°C - 1100°C to achieve the required flux.

After 10 to 15 minutes, the oven temperature equilibrated, the beam equivalent pressure (BEP) was measured, and the setpoint was either raised or lowered. This procedure was repeated until the growth flux of 0.8 - 1.2 x 10^{-6} Torr was atained. At this point, the substrate was rotated into the growth position, the surface reconstruction was checked with RHEED to ensure it had not changed, the substrate rotation was set to 10 RPM, and the flux was initiated.

After growth, the power to the substrate heater was shut off to minimize preferential desorption of sulfur from the surface. The substrate holder assembly was rotated out of position, and the shutter to the ZnS oven was briefly opened to measure the ZnS BEP.

This value usually did not differ from the initial value by more than 0.1 x 10^{-6} Torr (<15%). Once the value of T_{sub} dropped below 125°C, the substrate was transferred from the growth chamber to the Auger analysis chamber or to the load lock for removal. The elastic peak at 2000 eV was found, and an energy spectrum scan was performed from 0 to 2000 eV. The Zn and S peak heights were then measured for the sample and for a bulk sample.

Several different procedures were also investigated during this study for enhancing layer quality, as assessed by RHEED, because they had been found to be effective in the growth of other II-VI compounds such as CdTe and ZnTe. These were: dropping T_{sub} under a ZnS flux, applying a temperature pulse of about 50°C to the substrate for about 1 minute; and ramping up T_{sub} and/or the flux level after film nucleation. The reasoning behind these procedures was to increase the surface mobility and/or lattice energy to enhance crystallinity. However, when these techniques were used, twinning was seen in the RHEED patterns. A simpler procedure that seemed to produce better RHEED patterns consisted of using lower values of T_{sub} and a preset flux level which remained nearly constant throughout the run.

During the initiation of film growth, the formation of spots (island growth) and the transformation from spots to streaks (layer-by-layer growth) was observed continuously with RHEED. Photographs were taken just before growth, and after 5, 15, 30 and 45, and 60 minutes of flux. Growth periods were normally about 2 hours.

As previously discussed, the measured temperatures may differ from the actual substrate surface temperature by as much as 125°C. Given the results reported in the literature, it is suspected that the temperatures measured may be less than the actual temperatures. Some studies have reported optimal growth temperatures for ZnS on (100) Si as 340°C.[4] It was determined that for the range of relative temperutres studied (200-340°C) that the best results were

obtained for the lower values of T_{sub}: 200-240°C. This is suggested by comparing the RHEED patterns for runs 87-7 and 87-13. It can be seen that a transition is made from the island-growth mode to the Stranski-Krastanov growth mechanism as evidenced by Figures 12b and 12c after 1 hour, 50 minutes of flux at 280°C. The pattern, however, still has considerable contrast variation along the streaks (arrowheads) indicating the surface was not smooth. This may be due to some faceting of the layer - the substrate temperature is simply too high in this case. By comparison, run 87-13 was performed at a comparable flux, but at a much lower T_{sub} = 200°C. Here, more uniform steaking is seen in Figure 13 even after only 30 minutes. This suggests a smoother surface and a more stoichiometric layer.

While this set of data indicates that a colder substrate is preferable, there is certainly a lower limit. While the sticking coefficients for both zinc and sulfur should increase as T_{sub} drops, surface mobility will decrease. There is, then, a tradeoff of these two parameters which must be balanced.

To obtain accurate measurements of the growth rate, half of the layer was protected with black wax and the remainder was removed by etching in a solution of 50% HCl and 50% DI H_2O. Film thickness was measured on a step-profilometer. Three measurements were taken along the diameter of the wafer. Averages at each point were found as well as the average of the three positions along the diameter. The resulting growth rates were all slightly greater than 1/3 micron per hour.

RHEED Studies

Following the previous described study, a second set of samples was grown and evaluated. Table 3 lists the conditions of this study. During growth, the crystallinity of the films were evaluated by in-situ observation of RHEED patterns. A variety of

ORIGINAL PAGE
BLACK AND WHITE PHOTOGRAPH

a) RHEED after 5 min. flux (= 1.2×10^{-7} torr) T_{sub} = 200°C

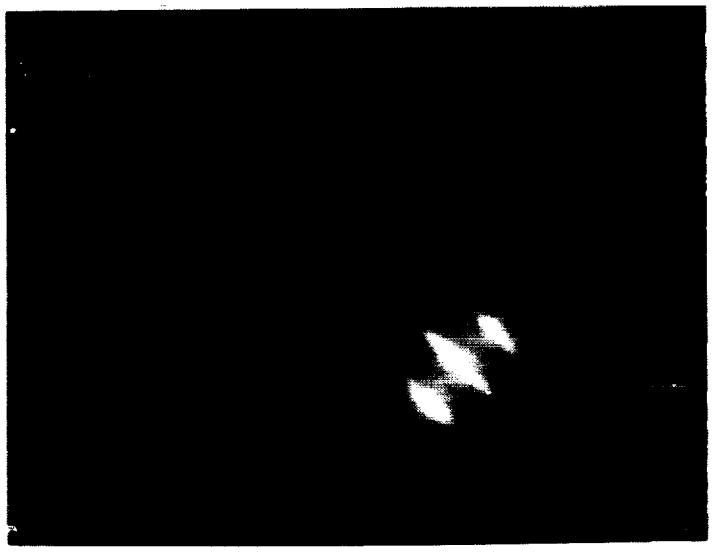

b) RHEED for T_{sub} = 200°C after 30 min. at flux. RHEED indicates a smooth film

Figure 13. RHEED studies for Layer 87-B.

Table 3. Experimental Parameters for Second Set of ZnS Growth Runs. Desorption Temperature, Substrate Temperature and Flux.

SAMPLE	FINAL DESORP. TEMP.(C)	TIME @ TEMP. (MIN)	Tsub @ FLUX INITIATE	Tsub FOR GROWTH (C)	TEMP. PULSE?	FLUX INIT./FIN (x10-7 TO
88-1	1000	13	300	300	YES	2.0/?
88-2	1000	>30	450	278	YES	12.0/11.4
88-3	950	57	350	350	YES	5.8/?
88-4	850	15	300	200/260	NO	5-11/10.2
88-5	850	32	300	150/200	YES	5-11/?
88-6	850	47	100	125	YES	9.2/9.4
88-7	850	~15	116	116	NO	8.8/8.2
88-8	850	25	100	100/57	NO	10/9.8
88-9	850	25	100	100/87	NO	10/10
88-10	850	13	100	100	NO	10.4/9.6
88-11	925	14	90	?	NO	9.8/?
88-12	775	8	90	90	NO	9.8/11
88-13	450/375	64/63	200	200	NO	0.33/10.2
88-14	850	13	150	150	NO	8/9.4
88-15	850	3	175	175	NO	9/9.2

film morphologies was also observed for these samples over a large substrate temperature range (57°C-350°C). Films grown at low temperatures were polycrystalline or amorphous, whereas those grown at the upper end of the temperature range were polycrystalline or twinned. For the best films, a transition from the (2x2) reconstruction pattern of the bare Si surface to a (1x1) streaky pattern indicated a smooth surface and layer-by-layer growth. These films were grown at temperatures of 100°C, 116°C, 150°C and 175°C.

Significant streak broadening occurred as soon as 15 minutes after flux initiation and increased until growth was terminated (Figure 14). This broadening was attributed to either 2-dimensional disorder arising from the formation of antiphase domains as the film grows, or to a high dislocation density. RHEED patterns for several samples also exhibited evidence of twinning. As shown by Figures 15 and 16, twinning is indicated by spots on either side of a primary streak in a crystalline RHEED pattern or as excess spots in a polycrystalline pattern. Twinning in (100)-oriented ZnS and ZnSe typically results in a change from a <100> orientation to two <511>-substrate directions growing on two (111) planes.[27] Twin formation also occurred in a film grown on a (111)-oriented Si substrate (Figure 17), where it is more difficult to nucleate a stable film, because there is only one bond extending from the lower half of the biatomic ZnS layer to the Si surface. It was found that most twinned films occurred when either high oxide desorption temperatures or high T_{sub} were used.

In general, a pattern indicating a polycrystalline or amorphous structure was the result of either: 1) poor predeposition conditions due to incomplete removal of oxide, carbon contamination or surface roughness or 2) low surface mobility due to low T_{sub}. At low temperatures, the difference in the Zn and S vapor pressures becomes more pronounced.

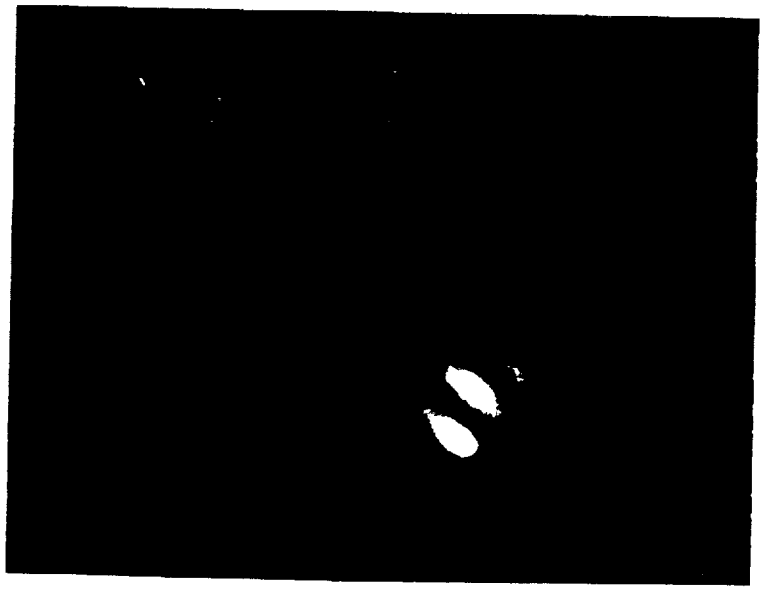

Figure 14. Streak Broadening Occurs as Growth Progresses.

ORIGINAL PAGE
BLACK AND WHITE PHOTOGRAPH

ORIGINAL PAGE
BLACK AND WHITE PHOTOGRAPH

Figure 15. Twin Spots in a Single Crystal RHEED Pattern.

ORIGINAL PAGE
BLACK AND WHITE PHOTOGRAPH

Figure 16. Twin Spots in a Polycrystalline RHEED Pattern.

ORIGINAL PAGE
BLACK AND WHITE PHOTOGRAPH

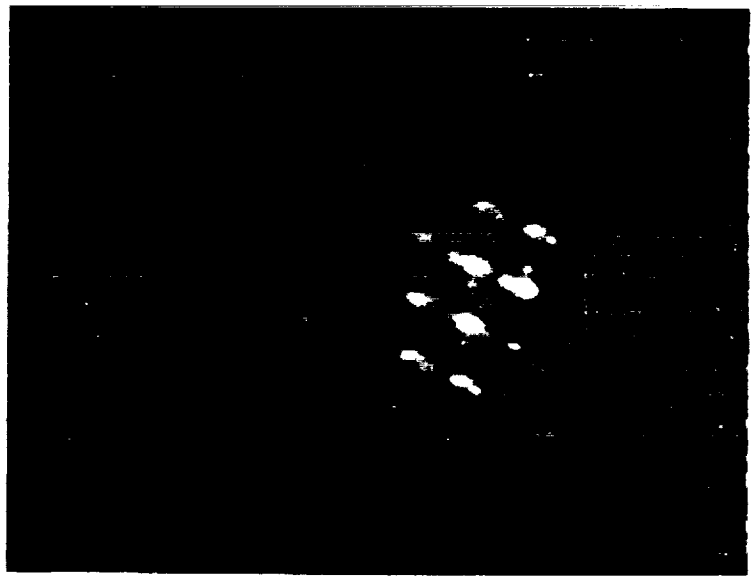

Figure 17. Twinning in a ZnS Film Growing on a Si(111) Substrate.

The number of site changes between impingement and desorption that either S or Zn can make at 100°C are calculated to be no more than 16 and 0.002 for S and Zn, respectively. This means there is little chance the atoms will have time to reach their equilibrium positions before being buried by the next layer.

The transition temperature, between single crystal and polycrystalline structures, was difficult to isolate. In the case of sample 88-8, after 5 minutes of flux at T_{sub} = 100°C, the power to the substrate heater was cut off and the temperature was allowed to decay. After 30 minutes of flux, the temperature had fallen by 30 degrees, but polycrystalline rings were not yet prominent. Even at 57°C arrowheads were visible, but not rings. From the growth conditions examined in this study, it would seem that a T_{sub} of 100°C was the lower limit in achieving single crystal growth.

In summary, while varying degrees of long and short-range order were observed with RHEED, the clearest streaks were seen in samples 88-14 and 88-15 with T_{sub} of 150° and 175°C, respectively. Amorphous structures resulted from nucleation at substrate temperatures below 100°C due to insufficient surface mobility. Twinning was prevalent in films grown above 175°C. The majority of these films (88-1 through 88-5) were grown on substrates that had been subjected to a high-temperature thermal cleaning which is known to cause surface roughness. These surface protuberances served as twinning sites.

X-Ray Diffraction Measurements

Double Crystal Rocking Curve (DCRC) measurements were made on all specimens to identify which substrate temperatures produced the films of highest quality (i.e., the lowest dislocation density). Only four of the films had detectable peaks from the ZnS layer, and they were quite broad (>2700 arc-sec).

The breadth of these DCRCs may be explained by a high dislocation density in the epilayer. The dislocation density, n_α,

may be calculated from the following equation:

$$N_\alpha = \beta_\alpha^2/4.35b^2,$$

where β_α is the FWHM due to lattice tilting and b is the Burger's vector.[28] For a cubic crystal like ZnS, the smallest possible b value is $a/\sqrt{2}$. From this equation, the narrowest peak of 2700 arc-sec corresponds to a dislocation density of $3 \times 10^{10}/cm^2$.

Auger Electron Spectra

In-situ Auger electron spectroscopy (AES) was performed immediately following growth to establish the relative stoichiometric ratios by computing the sulfur to zinc peak height ratio for each sample. These spectra were then compared with the spectrum obtained from a sputtered bulk ZnS sample. The S:Zn ratios for the MBE-deposited films was between 22% and 33%, while the ratio for the sputtered bulk sample is nearly 49%. The much larger sulfur to zinc ratio in the bulk sample suggests that the deposited films have less than the stoichiometric amount of sulfur present. An Auger spectrum was also obtained from an amorphous sample grown at room temperature where the sticking coefficient for each constituent is unity. This sample 88-8 closely approximates the sulfur to zinc ratio of the sputtered bulk sample (46%). Additionally, the Auger spectrum from a sample grown with T_{sub} 300°C, showed no measurable amount of sulfur stuck to the surface. Thus, the non-stoichiometry is identified with a less than unity sticking coefficient for S at growth temperatures between 100-200°C.

Conclusions of MBE ZnS Growth Study

RHEED results showed twinning occurred if T_{sub} was too high. Twinning occurred for two reasons: 1) the oxide desorption temperature had been high (samples 88-1 through 88-3) and induced

a rougher surface, or 2) T_{sub} had been high, causing preferential sulfur desorption. In a fairly narrow temperature range (150°C - 175°C) films initially grew as single crystals, as demonstrated by a transition from the (2x2) reconstruction pattern of a clean Si surface to a (1x1) pattern for the ZnS overlayer. However, as growth proceeded, streak broadening occurred and indicated disorder in the film. This disorder is attributed to the high dislocation density and the presence of antiphase domains. At very low substrate temperatures (<100°C), RHEED showed the films to be amorphous or polycrystalline. Amorphous films were the result of insufficient adatom surface mobility where Zn and S atoms did not have sufficient energy to sample their lowest energy positions.

DCRCs could not be obtained for most films. Only four of the samples had DCRCs that could be measured with reasonable accuracy. The narrowest of these peaks was found to have a FWHM value of 2700 arc-sec. This, again, is an indication of disorder in the film. If only dislocations caused the broadening, the minimum dislocation content is estimated to be $3 \times 10^{10}/cm^2$, which is very high.

The growth rate for the thin films grown between 57°C and 175°C was ≈1/3 μm/hr (0.27-0.37 μm/hr). The optimum growth rate as given by Yokoyama, et al. is 0.18 μm/hr.[27] It is possible that the fluxes used in these experiments ($8-12 \times 10^{-7}$ Torr) were too high. This may have resulted in a condition where the atom arrival rate is much shorter than the average residence time ($\Delta t << t_{res}$) and may have caused a transition from a layer-by-layer growth mode to a Stranski-Krastanov growth mode. If there were too many independently nucleated islands coalescing, antiphase boundaries would have formed. The resulting structure would explain why the samples had broad RHEED streaks and broad DCRCs. Further experiments should aim at holding T_{sub} constant at about 150°C and at varying the total flux level.

The Auger spectra suggest that the films did not deposit stoichimetrically. This was seen in the ratio of sulfur the zinc

peak heights. The deposited films have smaller sulfur to zinc peak height ratios than either the bulk sample or the polycrstalline film 88-8 in which T_{sub} = 57°C. Of all the deposited films for which Auger peaks were taken, sample 88-8 had the lowest substrate growth temperature, and it was therefore expected that this sample would be polycrystalline or amorphous, and have an Auger peak height ratio similar to the bulk sample.

In summary, a range of substrate temperatures produced a range of ZnS thin film morphologies which were characteristic of different growth kinetics. At low T_{sub} (<100°C), amorphous and polycrystalline films were the result of lowered surface mobility. At high T_{sub} (>175°C), twinning was common. This may have been due to preferential sulfur desorption as indicated from AES results. In an intermediate temperature range, single crystal deposits were observed with RHEED. These films exhibited reduced periodicity and high dislocation density as indicated by RHEED and x-ray DCRCs, respectively.

Though an "optimum" T_{sub} was found, the predetermined source flux may have been suboptimal. Indeed, the use of a single compound effusion source made it impossible to supply an overpressure of either Zn or S. Future experimental techniques which vary total source flux levels and J_{Zn}/J_S ratios are described in the next chapter.

3.7 Chemical Beam Epitaxy System Development

The development of a CBE growth system was undertaken to address the problems encountered in the growth of ZnS on Si by MBE. The advantages of this approach have implications for the cleaning and growth of ZnS and other II-VI compounds such as ZnSe, ZnTe and superlattices. The use of gas sources can aid in desorbing oxide from the Si surface and in controlling the individual constituent pressure ratios.

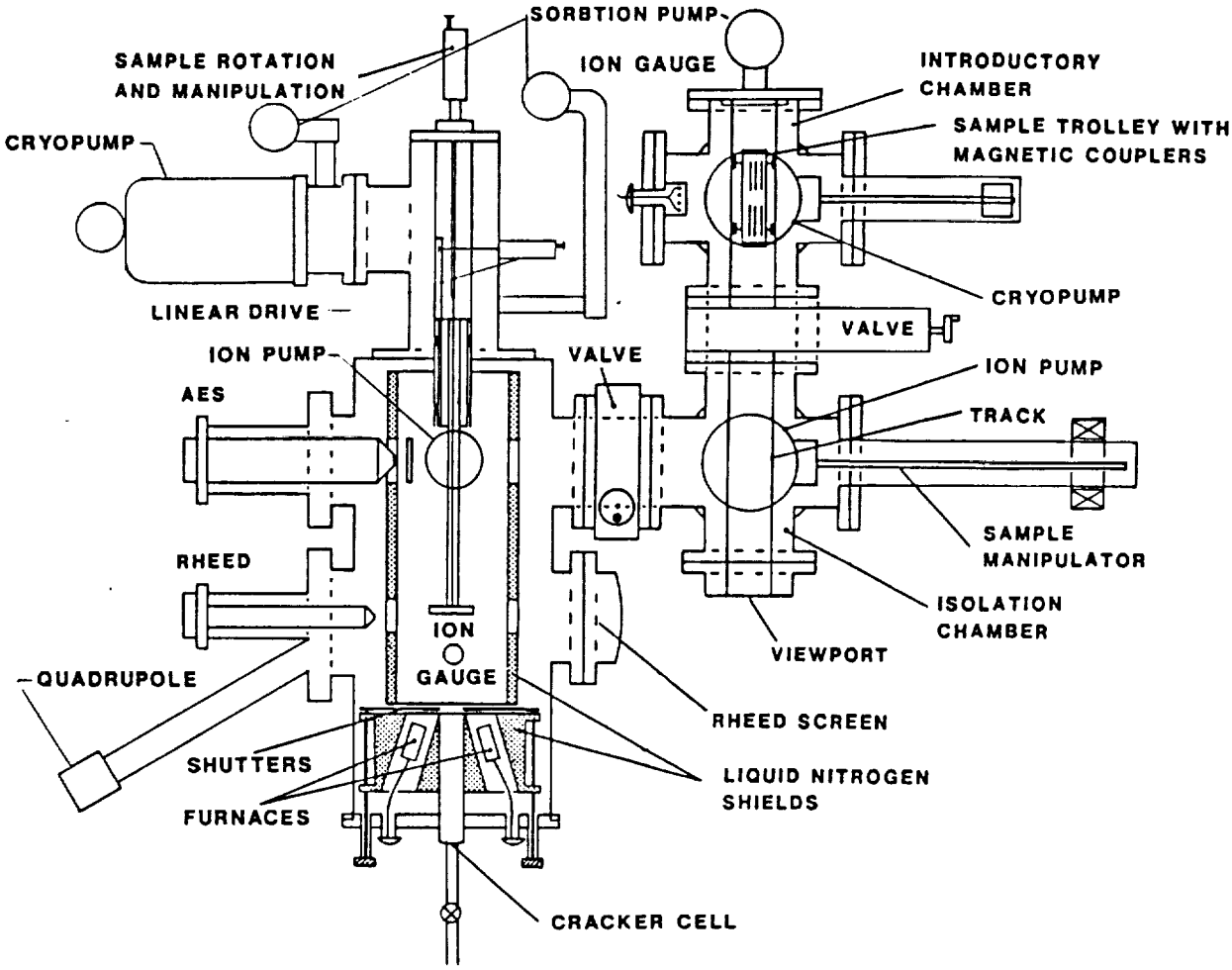

Figure 18. Schematic of Developmental Chemical Beam Epitaxy System.

The system, a schematic of which is shown in Figure 18, consists of three separate chambers: a load lock, a transition chamber and a growth chamber. The load lock is equipped with a sorption pump and a CryoTorr CT-100 cryopump. The transition chamber vacuum is maintained by a Varian VacIon ion pump with a pump speed of 220 liters/sec. The growth chamber is pumped by a CryoTorr CT-8 cryopump and another ion pump with pumping speeds of 1100 and 440 liters/sec, respectively. Two sorption pumps are used to lower system pressurrre from near atmospheric (70 Torr) to 10^{-4} Torr. One sorption pump is connected directly to the growth chamber, the other is located between the cryopump and a gate valve on the growth chamber. This enables purging and regeneration of the cryopump without the loss of growth chamber vacuum. Pressure in the growth chamber is measured by two nude ion gauges: one at the chamber wall, and one which may be moved in and out of the beam flux. There is also an ion gauge in the load lock, and in the transition chamber. In-situ analytical capability consists of RHEED, AES and a quadrupole mass spectrometer. The mass spectrometer is useful in optimizing the design and operation of any gas source cracker. The source flange consists of six receptables suitable for holding six solid source crucibles or gas injectors. The current configuration has crucibles for holding solid ZnS, Zn, Se or Mn.

For the initial configuration, H_2S gas is supplied through a port at the center of the source flange. H_2S gas serves two purposes. First, the sulfur will be used to help volatilize the surface oxide on the Si substrate according to the reaction:

$$SiO_2 + 2H_2S \rightarrow Si + 2SO + 2H_2.$$

Yongnian et al. report removing the silica complex at temperatures as low as 450°C.[29] This is a significant reduction from the 850°C-1100°C temperatures required in the MBE system, and should

significantly reduce the generation and migration of defects on the surface caused by high temperature thermal cleaning. A successful low-temperature technique for Si oxide removal is crucial for developing a viable heteroepitaxial growth capability. In addition, low-temperature oxide removal would allow the use of indium for bonding Si wafers to molybdenum substrate holders. Second, the H_2S gas will serve as the initial source of zinc (to be converted later to a metalorganic zinc source such as DEZ). With this configuration, the flux for Zn and S can be individually and precisely regulated, and the J_{Zn}/J_S ratio may be varied.

An H_2S cracking cell has been developed that consists of an alumina tube with a tantalum resistance coil. A tungsten-rhenium thermocouple is attached to the outside of the tube, and the entire tube is wrapped in tantalum foil for thermal isolation. The cracking tube is connected to the H_2S source by electropolished stainless steel tubing. The gas delivery tube contains a Unit Instruments model 1201 MFC and a Nupro BK series valves for isolation and purging.

Figure 19 shows the vapor pressures for the various molecular species of sulfur with respect to the vapor pressure of ZnS. This Figure shows the vapor pressures of zinc and sulfur are both higher than that of ZnS for a given temperature. Also, the sticking coefficients for S and S_2 are very different, and therefore, the growth mechanisms will be different. From this thermodynamic data, the equilibrium constants for the reactions may be determined. According to this data H_2S cracks into H_2 and S_2 at around 500°K, and further dissociates into H and S at around 1000°K. Also, varying the inlet pressure of H_2S, a ratio of S/S_2 molecular beam intensities can be selected.[30] Thus, the cracker was designed so as to produce the desired ratio of sulfur molecular species.

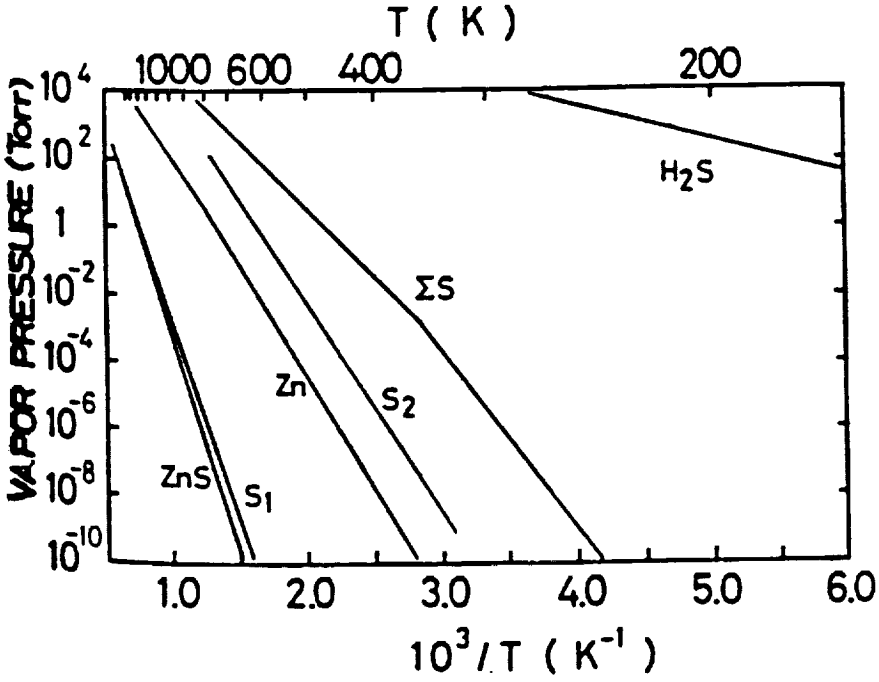

Figure 19. Vapor Pressure of Sulphur Species of Molecular Beam Epitaxially Grown ZnS.

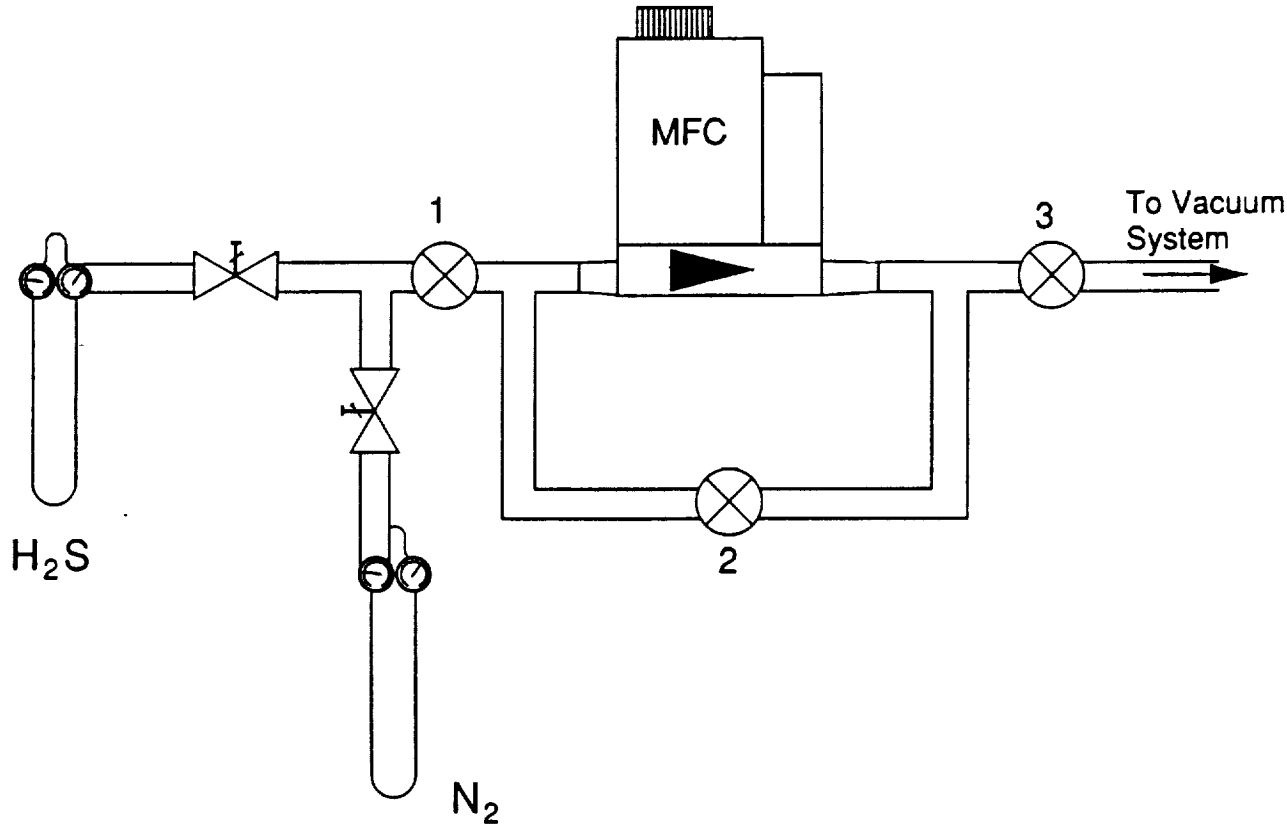

Figure 20. Schematic of CBE Gas Delivery System.

CBE Gas Delivery System Calibration

The initial calibration of the gas delivery system was performed with ultra-high purity N_2. Figure 20 shows the configuration of this system. All three Nupro air-actuated valves were in the normally closed position. All three valves were then opened to evacuate the line up to the needle valve on the low-pressurre side of the N_2 tank valve. Valves 1 and 2 were then closed. The low-pressure side of the tank valve was set to an arbitrarily low value of 5 to 10 psi. The needle valve was then opened. Valve #1 was then opened and the pressure upstream of the MFC was then at 5 to 10 psi. The needle valve was then closed. A sufficient reservior of N_2 exists between the needle valve and the MFC to ensure repeatability during calibration. (Only 50 Torr is requiired on the upstream side of the MFC.) If this were an actual source gas to be used during a growth run, the needle valve would be left open.

4. CONCLUSIONS

In this program a study has been made of thin-film electroluminescent devices since they offer a possible means of achieving a high resolution, light weight, compact video display panel for computer terminals or television screens. Unfortuantely, electroluminescent, EL, devices are at present highly inefficient, and can be made reliably to emit only in a few colors. Nevertheless, EL devices offer significant advantages over other existing technologies such as cathode ray tubes, plasma and liquid crystal displays.

A review of these devices showed that the performance of any EL device, either ac or dc, depends upon the probability of an electron impact exciting a luminescent center which in turn depends upon the density of centers present in the semiconductor layer, the probability of an electron achieving the impact excitation threshold energy and the collision cross section itself. Present EL devices exhibit very poor overall efficiencies due to several reasons. First, the number of luminescent centers cannot be effectively increased much beyond 1-2% in concentration without causing quenching. Secondly, the collision cross section, which is an inherent property of the center, cannot be readily engineered. Therefore, the efficiency can best be improved by increasing the number of hot electrons capable of impact exciting a center.

Studies were therefore directed toward calculating the hot electron distributions in ZnSe and ZnS. This showed that because of the larger electron scattering rate of electrons in ZnS, due to the higher polar optical phonon energy and electron effective mass, very few electrons were "heated" to energies in excess of 2.3 eV as is required to impact-excite a Mn luminescent center. For ZnSe the number of electrons gaining an energy of 2.3 eV or greater was

estimated to be larger at ~2-3%. Because the generation of a high density of hot electrons was identified as representing a major limitation to the efficiency of thin-film electroluminescent devices, new concepts for achieving a high concentration of hot electrons were investigated. As a consequence of these studies, we invented a novel variably spaced superlattice energy filter (VSSEF) device which provides a high energy injection of near monoenergetic electrons into a bulk semiconductor layer at an energy tuned to the impact-excitation energy of the luminescent center. This concept is projected to produce a dramatic increase in the efficiency and brightness of TFEL devices with the additional advantage of low voltage dc operation. Thus, the operating conditions required for this device could make it compatible with silicon integrated circuits. To fully explore the utility of this concept, a theoretical formalism of the energy level scheme and resonant tunneling characteristics of variably spaced superlattice structures in an electric field was developed and used to model a possible EL device structure. This concept was also experimentally demonstrated in coupled two- and three-well variably spaced AlGaAs/GaAs superlattices grown by MBE. In these structures resonant tunneling and negative differential resistance effects were observed for the first time.

In conjunction with the above studies, growth studies were also performed and ZnS was grown by MBE on both (001) GaAs and (001) and (111) Si substrates. The ZnS epitaxial layers on GaAs were grown by using both low and high temperature nucleation techniques. RHEED analysis of the layers grown using both techniques indicated that high temperature nucleation gave the smoother ZnS surfaces, but the DCRC results were insensitive to the nucleation temperature. Typical FWHM values ranged from 1200 to 800 arc second for layer thickness between 0.4 and 2.4 μm. In general, the results showed that the quality of the ZnS layers were critically dependent on the initial roughness of the GaAs surface.

Thin films of zinc sulfide were also deposited by molecular beam epitaxy (MBE) on (100) and (111)-oriented silicon. The wafers were cleaned with a standard RCA-type procedure and mounted on molybdenum blocks without the use of indium solder. The films were characterized by RHEED, AES, X-ray DCRC, and step-profilometry.

RHEED patterns indicated single crystal, polycrystalline and amorphous films were grown over a temprature range of 57 to 350°C at a constant flux level. X-ray DCRCs yielded very large full-width at half-maximum (FWHM) values, suggesting a high dislocation density or the formation of antiphase domains. AES data indicated the films may be sulfur deficient. These results suggest that using a single compound effusion source cannot guarantee stoichiometry in the arriving flux.

Chemical Beam Epitaxy (CBE) offers several advantages over MBE in fabricating new device structures. Consequently, a new growth system has been designed and built which will use H_2S gas as a sulfur source and two solid sources of zinc and zinc sulfide. This system will allow source constitutent pressure ratios to be varied. Using H_2S will also enable the removal of surface oxide at low temperatures.

It should be noted that while much work has been presented on the growth of ZnS and ZnSe on GaAs by MOCVD, there are relatively few reports of MBE growth of ZnS on Si. ZnS, being a polar material, is difficult to grow on Si, which is non-polar. In addition, ZnS has a relatively high melting temperature and high vapor pressure. Flux reproducibility is, therefore, difficult. Using a single, solid compound source, the flux ratio of the impinging species is fixed. It is not possible to provide an overpressure of either Zn or S with this source. The use of indium solder as a means for securing the wafer to the molybdenum holder also presents a problem for Si wafers. The oxide desorption temperature for Si is around 800°C. At this temperature, the indium quickly desorbs causing contamination of the substrate. The

development of an indium-free mounting technique was therefore essential for high-temperature thermal cleaning. However, it is also possible that the use of H_2S as a sulfur source may provide a low-temperature method for desorbing the oxide from Si, and thus provide another reason for a CBE approach.

The difficulty in obtaining good films can be also attributed to the kinetics of growing zincblende on a diamond structure. These fundamental difficulties include interface charge imbalance and antiphase disorder.[25] ZnS is strongly ionic, with an ionicity value f_i of 0.623, while Si is not.[26] For a stable layer to form, the lower atomic layer of the first biatomic (monomolecular) layer must contain only sulfur atoms on the silicon surface. The second layer should contain only zinc atoms. This is for two reasons: 1) the Zn-Si bond is not energetically favorable for chemical reasons, and 2) each sulfur atom has two bonds with the silicon atoms and two bonds with the zinc atoms. For epitaxial growth on a (111)-oriented Si surface, there is only one bond extending from the sulfur atom to the silicon atoms, and three bonds extending to the zinc layer. The single bond means that it is more difficult to maintain a perfect interface without inducing disorders such as twins. Heteroepitaxy is therefore favored on Si(100) substrates,[27,28] as demonstrated by our results.

5. TECHNICAL PRESENTATIONS AND PUBLICATIONS

During the period of this contract, the following presentations, publications and patent applications were generated.

Presentations

1. The Variably Spaced Superlattice Energy Filter, C.J. Summers, B.K. Wagner, H.D. Rodgers, and K.F. Brennan, Second International Conference on Superlattices and Microstructures, Goteburg, Sweden, July 1986.

2. Resonant Tunneling and Negative Differential Resistance in Variably Spaced Superlattice in the AlGaAs/GaAs System, C.J. Summers, K.F. Brennan, A. Torabi, H.M. Harris, and J. Comas, Third International Conference on Modulated Semiconductor Structures, Montpellier, France, 6-11 July 1987.

3. Molecular Beam Epitaxial Growth and Structural Characterization of ZnS on (001) GaAs, R.G. Benz II, P.C. Huang, S.R. Stock, and C.J. Summers, Third International Conference on II-VI Compunds, Monterey, California, 12-17 July 1987.

Published Papers

1. "Variably Spaced Superlattice Energy Filter, A New Design Concept for High-Energy Electron Injection," by C.J. Summers and K.F. Brennan, Appl. Phys. Lett. 48, 806-808 (1986).

2. "Theory of Resonant Tunneling in a Variably Spaced Multiquantum Well Structure: An Airy Function Approach," by K.F. Brennan and C.J. Summers, J. Appl. Phys. 61, 614 (1987).

3. "The Variably Spaced Superlattice Energy Filter," by C.J. Summers, K.F. Brennan, H.D. Rodgers and B.K. Wagner. Presented at the 2nd Int. Conf. on Superlattices and Microstructures, Sweden, 1986. Published in Superlattices and Microstructures 3, 147-152 (1987).

4. "The Variably Spaced Superlattice Electroluminescent Display: A New High Efficiency Electroluminescence Scheme," by K.F. Brennan and C.J. Summers, J. Appl. Phys. 61, 5410-5418 (1987).

5. "Molecular Beam Epitaxial Growth and Structural Characterization of ZnS Layers Grown on (001) GaAs," by R.G. Benz, P.C. Huang, S. Stock, and C.J. Summers. J. Crystal Growth 86, 303-310 (1988).

6. "Theory of High Field Electronic Transport in Bulk ZnS and ZnSe," K.F. Brennan, J. Appl. Phys. 64, 4024-4030 (1988).

7. "Characterization of ZnS Film Grown on Si(100) by Molecular Beam Epitaxy," J.A. Goldman, Masters Thesis, Georgia Institute of Technology (1988).

Patent Applications

1. Variably Spaced Superlattice Energy Filter, C.J. Summers and K.F. Brennan.

2. Improved Detectors Which Use a Variably Spaced Superlattice, K.F. Brennan and C.J. Summers.

6. TECHNICAL PERSONNEL

The technical personnel who contibuted to this project were:

Dr. Christopher J. Summers

Dr. Kevin Brennan

Mr. Brent K. Wagner

Mr. Rudy Benz II

Mr. Jonathan Goldman

All of these investigators are with the Georgia Institute of Technology.

7. REFERENCES

1. R. Mach and G.O. Muller, Physical Concepts of High-Field, Thin-Film Electroluminescence Devices, Phys. Stat. Sol. (a) 69, 11-66 (1982).

2. S. Smith, International Workshop on Electroluminescence, Liege, 1980, J. Lum.

3. D.A. Cuseno, Luminescence of Organic and Anorganic Materials, Ed. Kallman and Spruch, Wiley, NY (1962).

4. T. Mishima, W. Quan-Kun and K. Takahashi, J. Appl. Phys. 52, 5797-5799 (1981).

5. R. Mach, W. Gericke, H. Trepton and W. Ludwig, Phys. Stat. Sol. (a) 49, 667 (1978).

6. H.E. Gumlich, Sammlung, Vieweg. Branschweig, 1970.

7. H.E. Gumlich, R.L. Pfrogner, J.C. Shafer and F.E. Williams, J. Chem. Phys. 44, 3929 (1966).

8. K. Brennan, J. Appl. Phys. 64, 4024-4030 (1988).

9. C.J. Summers and K.F. Brennan, Appl. Phys. Lett. 48, 806 (1986).

10. M. Aven and B. Segall, Phys. Rev., 130, 81 (1963).

11. H.E. Ruda, J. Appl. Phys., 59, 1220 (1986).

12. H.E. Ruda, J. Appl. Phys., 59, 3516 (1986).

13. J. Shah and A.E. DiGiovanni, Appl. Phys. Lett., 33, 995 (1978).

14. F. Capasso, Lightwave Communications Technology, edited by W.T. Tsang, Vol. 22, Part D of Semiconductors and Semimetals, edited by R.K. Willardson and C.C. Beer (Academic, NY) 1985, p. 1.

15. R. Mach and G.O. Muller, Phys. Status Solid A, 69, 11 (1982).

16. F. Williams, J. Lumin., 23, 1 (1981).

17. M. Heiblum, Solid-State Electron., 24, 343 (1981).

18. T.C.L.G. Sollner, W.D. Goodhue, P.E. Tannenwald, C.D. Parker, and D.D. Peak, Appl. Phys. Lett. 43, 588 (1983).

19. T.C.L.G. Sollner, E.R. Brown, W.D. Goodhue and H.Q. Le, Appl. Phys. Lett., 50, 333 (1987).

20. K.F. Brennan and C.J. Summers, J. Appl. Phys., 61, 614 (1987).

21. C.J. Summers, K.F. Brennan, A. Torabi, and H.M. Harris, Appl. Phys. Lett., 52, 132 (1988).

22. C.J. Summers, K.F. Brennan, A. Torabi, H.M. Harris, and J. Comas, Journal de Physique, C-5 Supplement 11, 457 (1987).

23. C.J. Summers, K.F. Brennan, H.D. Rodgers, and B.K. Wagner, Superlattices and Microstructures 3, 147-152 (1987).

24. A.J. SpringThorpe, S.J. Ingrey, B. Emmerstorfer, P. Mandeville and W.T. Moore, Appl. Phys. Lett., 50, 78 (1987).

25. D. Theis, H. Oppolzer, G. Ebbinghaus and S. Schild, J. Cryst. Growth 63, 47-57 (1983).

26. R.C. Henderson, J. Electrochem. Soc. 119, 773 (1972).

27. M. Yokoyama, K. Kashiro and S. Ohta, J. Appl. Phys. 60, 350 (1986).

28. M.J. Hordon and B.L. Averbach, Acta Metallurgica 9, 238 (1961).

29. Y. Yongnian, C.F. Hickey and U.J. Gibson, Thin Solid Films 151, 209 (1987).

30. S. Kaneda, S. Satou, T. Setoyama, S. Motogama, M. Yokayama and N. Ota, J. Crystal Growth 76, 442 (1986).

APPENDIX A
PUBLISHED PAPERS